Studying ocean acidification with conservative, stable numerical schemes for nonequilibrium air-ocean exchange and ocean equilibrium chemistry

Mark Z. Jacobson

Department of Civil and Environmental Engineering, Stanford University, Stanford, California, USA

[1] A noniterative, implicit, mass-conserving, unconditionally stable, positive-definite numerical scheme that solves nonequilibrium air-ocean transfer equations for any atmospheric constituent and time step is derived. The method, referred to as the Ocean Predictor of Dissolution (OPD) scheme, is coupled with EQUISOLV O, a new ocean chemical equilibrium module based on the EQUISOLV II atmospheric aerosol solver. EQUISOLV O converges iteratively, but is unique because it is positive-definite and mass and charge conserving, regardless of the number of iterations taken or equations solved. Two advancements of EQUISOLV O were the development of a new method to initialize charge and a noniterative solution to the water dissociation equation. Here OPD-EQUISOLV O is used to calculate air and ocean composition and ocean pH among dozens of species in the Na-Cl-Mg-Ca-K-H-O-Li-Sr-C-S-N-Br-F-B-Si-P system. The modules are first used in a one-dimensional ocean/two-compartment atmospheric model driven by emission to examine the historic change in atmospheric CO_2 and ocean composition from 1751 to 2004 and the possible future change in CO_2 and ocean composition from 2004 to 2104. CO_2 estimates from the historic simulation compare well with the measured CO_2 record. Whereas surface ocean pH is estimated to have dropped from near 8.25 to near 8.14 between 1751 and 2004, it is forecasted to decrease to near 7.85 in 2100 under the SRES A1B emission scenario, for a factor of 2.5 increase in H^+ in 2100 relative to 1751. This "ocean acidification" is calculated to cause a nontrivial transfer of ammonia from the atmosphere to the ocean and a smaller transfer of hydrochloric acid, nitric acid, and sulfurous acids from the ocean to the atmosphere. The existence and direction of these feedbacks are almost certain, suggesting that CO_2 buildup may have an additional impact on ecosystems. Computer time of the module in the GATOR-GCMOM global model with a 10-layer-ocean was less than two hours per simulation year on a modern single processor.

Citation: Jacobson, M. Z. (2005), Studying ocean acidification with conservative, stable numerical schemes for nonequilibrium air-ocean exchange and ocean equilibrium chemistry, *J. Geophys. Res.*, *110*, D07302, doi:10.1029/2004JD005220.

1. Introduction

[2] Air-ocean exchange is a mechanism of cleansing the atmosphere of gases and of injecting dissolved gases from the ocean back to the air. Exchange is one of the main removal mechanisms of atmospheric ozone [e.g., *Galbally and Roy*, 1980; *Chang et al.*, 2004] and carbon dioxide [e.g., *Stumm and Morgan*, 1981; *Butler*, 1982; *Liss and Merlivat*, 1986; *Wanninkhof*, 1992] and one of the main emission mechanisms of dimethylsulfide (DMS) [e.g., *Kettle and Andreae*, 2000].

[3] Of particular importance is the flux of carbon dioxide (CO_2) between the atmosphere and ocean. CO_2 has been increasing on a global scale due to anthropogenic emission,

and dissolution/dissociation/reaction in the oceans is a major mechanism of its removal. To date, models simulating the global carbon cycle have treated air-sea exchange of gases with a variety of methods. Some models have calculated the flux of CO_2 assuming a prescribed partial pressure of atmospheric CO_2 [e.g., *Sarmiento et al.*, 1992; *Caldeira and Wickett*, 2003]. Others have calculated the flux of CO_2 from the difference in modeled atmospheric partial pressure and measured ocean-surface CO_2 concentration, but have not tracked the change in concentration of the gas in the ocean or the feedback of its dissolution on ocean concentration or pH [e.g., *Olsen and Randerson*, 2004]. A third set of models has assumed a constant yearly CO_2 flux to the oceans [e.g., *Gurney et al.*, 2002; *Murayama et al.*, 2004]. A fourth set of models has assumed equilibrium between the ocean and atmosphere [e.g., *Brewer*, 1997]. A fifth set of models has calculated the

flux of CO_2 between the atmosphere and ocean explicitly but ocean equilibrium chemistry iteratively [e.g., *Maier-Reimer and Hasselmann*, 1987; *Maier-Reimer*, 1993a]. A final set has calculated the time-dependent fluxes either explicitly or iteratively [e.g., *Caldeira and Rampino*, 1993; *Jain et al.*, 1995].

[4] Many models have solved equilibrium equations in seawater [e.g., *Garrels and Thompson*, 1962; *Whitfield*, 1975a, 1975b; *Stumm and Morgan*, 1981; *Dickson and Whitfield*, 1981; *Turner et al.*, 1981; *Millero and Schreiber*, 1982; *Butler*, 1982; *Maier-Reimer and Hasselmann*, 1987; *Turner and Whitfield*, 1987; *Moller*, 1988; *Greenberg and Moller*, 1989; *Spencer et al.*, 1990; *Caldeira and Rampino*, 1993; *Clegg and Whitfield*, 1995; *Millero and Pierrot*, 1998]. Equilibrium models of atmospheric aerosols are also quite common [e.g., *Bassett and Seinfeld*, 1983; *Saxena et al.*, 1986; *Pilinis and Seinfeld*, 1987; *Kim et al.*, 1993; *Jacobson et al.*, 1996; *Nenes et al.*, 1998; *Jacobson*, 1999b; *Wexler and Clegg*, 2002; *Metzger et al.*, 2002; *Makar et al.*, 2003].

[5] Whereas, several models have simulated nonequilibrium ocean-atmosphere exchange of trace gases, all numerical solutions to date have either been explicit, thereby requiring a limited time step, or iterative, requiring more computational time. Currently, no solver of the transfer equations has been developed that is simultaneously implicit, noniterative, unconditionally stable, mass-conserving between the air and ocean, and positive-definite under all conditions. Here such a solution is given.

[6] In addition, whereas several analytical and iterative methods of solving ocean equilibrium exist, and the analytical solutions are positive-definite for solving a limited number of equations, no solver is positive-definite as well as charge- and mass-conserving regardless of the number of equations solved or number of iterations taken. Here, the unconditionally stable EQUISOLV II model that has been applied to atmospheric aerosols is adapted, with some improvement, to the ocean to produce EQUISOLV O.

2. Nonequilibrium Air-Ocean Exchange

[7] In this section, the method of solving air-ocean exchange is derived. The method is implicit, noniterative, unconditionally stable, mass-conserving, and positive-definite for any time step and species. It is analogous to the Analytical Predictor of Dissolution (APD) scheme derived for size-resolved aerosol particles in *Jacobson* [1997, 2002], but modified here for bulk ocean and atmosphere compartments rather than liquid drops. In addition, the solution derived here does not use exponentials, whereas the APD scheme did.

[8] The change in concentration of any gas q between the atmosphere and ocean due to surface dissolution and evaporation can be described with

$$C_{q,t} = C_{q,t-h} + \frac{hV_{d,gas,q}}{\Delta z_a}\left(\frac{c_{q,T,t}}{H'_q} - C_{q,t}\right) \quad (1)$$

where the subscripts t and $t - h$ indicate the current time and one time step backward, respectively, h is the time step (s), C_q is the atmospheric mole concentration of the gas

(mol cm^{-3}-air), $c_{q,T}$ is the mole concentration of the dissolved gas plus its dissociation products in seawater (mol cm^{-3}-water), $V_{d,gas,q}$ is the dry deposition speed of the gas (cm s^{-1}), Δz_a is the thickness of the atmospheric layer through which C_q is averaged (cm), and H'_q is a dimensionless effective Henry's constant (mol mol^{-1}). Equation (1) is written implicitly; thus, $c_{q,T,t}$ and $C_{q,t}$ are unknown in it. If the terms were written explicitly (with time subscript $t - h$) on the right side of the equation, the final concentration $C_{q,t}$ could become negative at a long time step or high deposition speed.

[9] The mole concentration of a gas is related to its partial pressure p_q (atm), by

$$C_q = \frac{p_q}{R^*T} \quad (2)$$

where R^* is the universal gas constant (82.058 cm^3 atm mol^{-1} K^{-1}) and T is absolute air temperature (K). The mole concentration (mol cm^{-3}) of a gas dissolved in seawater is related to the molality of the gas in seawater $\mathbf{m}_{q,T}$ (moles of dissolved gas plus its dissociation products per kilogram of dilute water) by
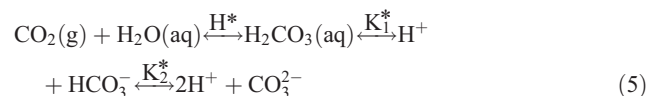
$$c_{q,T} = \rho_{dw}\mathbf{m}_{q,T} \quad (3)$$

where ρ_{dw} is the density of dilute water (kg cm^{-3}). Dilute water instead of seawater is used in this equation since molality is defined as the moles of solute per kilogram of solvent (water), not of solution (seawater). The temperature-dependent expression for the density of dilute water used here is

$$\rho_{dw} = \frac{A_0 + T_{w,c}\big(A_1 + T_{w,c}\big(A_2 + T_{w,c}\big(A_3 + T_{w,c}\big(A_4 + T_{w,c}\big(A_5 + T_{w,c}\big)\big)\big)\big)\big)}{1 + BT_{w,c}} \quad (4)$$

[*Kell*, 1972], where units of density are kg cm^{-3}, $T_{w,c}$ is water temperature (°C), $A_0 = 999.8396$, $A_1 = 18.224944$, $A_2 = -7.922210 \times 10^{-3}$, $A_3 = -5.5448460 \times 10^{-5}$, $A_4 = 1.497562 \times 10^{-7}$, $A_5 = -3.9329520 \times 10^{-10}$, $B = 18.159725$, and the valid range is 0–100°C.

[10] If a gas dissolves and dissociates twice in solution, as CO_2 does by the reactions,

$$CO_2(g) + H_2O(aq) \xrightleftharpoons{H^*} H_2CO_3(aq) \xrightleftharpoons{K_1^*} H^+$$
$$+ HCO_3^- \xrightleftharpoons{K_2^*} 2H^+ + CO_3^{2-} \quad (5)$$

then the dimensionless effective Henry's constant of the gas in seawater is

$$H'_q = \rho_{dw}R^*TH_q^*\left(1 + \frac{K_{1,q}^*}{\mathbf{m}_{H^+}}\left[1 + \frac{K_{2,q}^*}{\mathbf{m}_{H^+}}\right]\right) \quad (6)$$

where H_q^*, $K_{1,q}^*$, and $K_{2,q}^*$ are the Henry's Law coefficient (mol kg^{-1}-dw atm^{-1}) of CO_2 and the first and second dissociation coefficients (mol kg^{-1}-dw) of carbonic acid, respectively, all measured in seawater, and $\mathbf{m}_{H^+}$ is the molality (mol kg^{-1}-dw) of the hydrogen ion. The unit "mol kg^{-1}-dw" indicates that the coefficients have been converted, if necessary, from moles per kilogram of seawater to

moles per kilogram of dilute water, as discussed shortly. The seawater-measured rate coefficients implicitly account for the nonideality of solution.

[11] Three major methods exist to account for the non-ideality of seawater solutions. The first is to solve for activity coefficients with a specific ion interaction model [e.g., *Guggenheim*, 1935; *Leyendekkers*, 1972; *Pitzer*, 1973; *Whitfield*, 1975a, 1975b; *Harvie et al.*, 1984; *Pabalan and Pitzer*, 1987; *Moller*, 1988; *Greenberg and Moller*, 1989; *Spencer et al.*, 1990; *Millero and Hawke*, 1992; *Clegg and Whitfield*, 1995; *Millero and Pierrot*, 1998]. The second method is to solve for activity coefficients with an ion-pairing model [e.g., *Goldberg and Arrhenius*, 1958; *Sillen*, 1961; *Garrels and Thompson*, 1962; *Truesdell and Jones*, 1969; *Pytkowicz*, 1969; *Millero*, 1974; *Stumm and Morgan*, 1981; *Dickson and Whitfield*, 1981; *Butler*, 1982; *Millero and Schreiber*, 1982; *Millero and Hawke*, 1992; *Millero and Pierrot*, 1998]. The third method is to measure equilibrium rate coefficients in the medium of interest, thereby accounting for activity coefficients implicitly in the rate coefficients [e.g., *Mehrbach et al.*, 1973; *Hansson*, 1973; *Byrne and Kester*, 1974; *Weiss*, 1974; *Dickson and Millero*, 1987; *Goyet and Poisson*, 1989; *Roy et al.*, 1993; *Millero*, 1995]. In the case of the carbonate system, seawater rate coefficients (denoted with a *) are related to dilute-solution rate coefficients by

$$H_q^* = \frac{H_q}{\gamma_{CO_2(aq)}} \qquad K_{1,q}^* = \frac{K_{1,q}\gamma_{CO_2(aq)}}{\gamma_{H^+}\gamma_{HCO_3^-}} \qquad K_{2,q}^* = \frac{K_{2,q}\gamma_{HCO_3^-}}{\gamma_{H^+}\gamma_{CO_3^{2-}}}$$

(7)

where H_q is the Henry's Law constant of the gas in a dilute solution (mol kg^{-1}-dw atm^{-1}), $K_{1,q}$ and $K_{2,q}$ are the first and second dissociation constants, respectively, of the dissolved gas in a dilute solution (mol kg^{-1}- dw), and the γ's are single-ion solute activity coefficients.

[12] Here, the third method, using rate coefficients measured in seawater solutions, is used for the most important seawater reactions, namely those involving $CO_2(g)$ dissolution, and dissociation of CO_2-$H_2O(aq)$, NH_3-$H_2O(aq)$, $B(OH)_3(aq)$, $Si(OH)_4(aq)$, $H_3PO_4(aq)$, $HF(aq)$, $H_2S(aq)$, HSO_4^-, HCO_3^-, $H_2PO_4^-$, HPO_4^{2-}, and $CaCO_3(s)$. Table 1 gives the reactions corresponding to these processes and lists other dissolution and dissociation reactions treated here. The temperature- and salinity- or ionic-strength-dependent rate coefficients for the seawater-solution reactions are in nonstandard form and given in *Millero* [1995], except that the Henry's Law coefficient for $CO_2(g)$ dissolution and the first and second dissociation coefficients of carbonic acid are shown here:

$$\ln H_{CO_2}^* \left(\frac{mol}{kg - dw \, atm}\right) =$$
$$\cdot \left\{ \begin{array}{l} -60.2409 + 93.4517\left(\frac{100}{T_w}\right) + 23.3585\ln\left(\frac{T_w}{100}\right) \\ + S\left[0.023517 - 0.023656\left(\frac{T_w}{100}\right) + 0.0047036\left(\frac{T_w}{100}\right)^2\right] \end{array} \right\}$$

(8)

$$\ln K_{1,CO_2}^* \left(\frac{mol}{kg - dw}\right) =$$
$$\cdot \frac{\rho_{sw}}{\rho_{dw}} \frac{m_{H^+}}{m_{H^+,SWS}} \left(\begin{array}{l} 2.18867 - \frac{2275.0360}{T_w} - 1.468591\ln T_w \\ + \left(-0.138681 - \frac{9.33291}{T_w}\right)S^{0.5} + 0.0726483S \\ - 0.00574938S^{1.5} \end{array} \right)$$

(9)

$$\ln K_{2,CO_2}^* \left(\frac{mol}{kg - dw}\right) =$$
$$\cdot \frac{\rho_{sw}}{\rho_{dw}} \frac{m_{H^+}}{m_{H^+,SWS}} \left(\begin{array}{l} -0.84226 - \frac{3741.1288}{T_w} - 1.437139\ln T_w \\ + \left(-0.128417 - \frac{24.41239}{T_w}\right)S^{0.5} + 0.1195308S \\ - 0.00912840S^{1.5} \end{array} \right)$$

(10)

[*Millero*, 1995] (fitting to data from *Weiss* [1974] for equation (8) and to combined data from *Goyet and Poisson* [1989] and *Roy et al.* [1993] for equations (9) and (10)). In equations (8)–(10), T_w is the absolute temperature (K) of water, S is salinity (parts per thousand by mass), ρ_{sw} is the density of seawater (kg cm^{-3}), and

$$m_{H^+,SWS} = m_{H^+} + m_{HSO_4^-} + m_{HF} = m_{H^+}\left[1 + \frac{m_{SO_4^{2-}}}{K_{HSO_4^-}^*} + \frac{m_{F^-}}{K_{HF}^*}\right]$$

(11)

is the molality of total hydrogen ion (dissociated plus associated hydrogen ion) in solution based on the seawater scale (mol kg^{-1}-dw) [*Millero*, 1995]. The dissociation constants for the bisulfate ion and hydrofluoric acid in equation (11) are

$$K_{HSO_4^-}^* \left(\frac{mol}{kg - dw}\right) =$$
$$\cdot \left\{ \begin{array}{l} \frac{-4276.1}{T_w} + 141.328 - 23.093\ln T_w \\ + \left(\frac{-13856}{T} + 324.57 - 47.986\ln T_w\right)I^{0.5} \\ + \left(\frac{35,474}{T_w} - 771.54 + 114.723\ln T_w\right)I + \frac{-2698I^{1.5} + 1776I^2}{T_w} \end{array} \right\}$$

(12)

$$K_{HF}^* \left(\frac{mol}{kg - dw}\right) = 1590.2/T_w - 12.641 + 1.525I^{0.5} \qquad (13)$$

respectively [*Dickson*, 1990; *Dickson and Riley*, 1979; *Millero*, 1995], where

$$I = 0.5 \sum m_q z_q^2 \qquad (14)$$

Table 1. Equilibrium Reactions, Coefficients, and Coefficient Units[a]

Reaction		A	B	C	Units	Reference
Dissolution Reactions Used With Dissociation Reactions for Nonequilibrium Air-Ocean Transfer						
$O_3(g)$	$\Longleftrightarrow O_3(aq)$	1.13×10^{-2}	7.72		mol/kg-atm	C
$OH(g)$	$\Longleftrightarrow OH(aq)$	2.50×10^1	17.72		mol/kg-atm	E
$HO_2(g)$	$\Longleftrightarrow HO_2(aq)$	2.00×10^3	22.28		mol/kg-atm	E
$H_2(g)$	$\Longleftrightarrow H_2(aq)$	8.11×10^{-3}			mol/kg-atm	N
$H_2O_2(g)$	$\Longleftrightarrow H_2O_2(aq)$	7.45×10^4	22.21		mol/kg-atm	B
$NH_3(g)$	$\Longleftrightarrow NH_3(aq)$	5.76×10^1	13.79	-5.39	mol/kg-atm	A
$NO(g)$	$\Longleftrightarrow NO(aq)$	1.88×10^{-3}			mol/kg-atm	N
$NO_2(g)$	$\Longleftrightarrow NO_2(aq)$	1.00×10^{-2}	8.38		mol/kg-atm	D
$NO_3(g)$	$\Longleftrightarrow NO_3(aq)$	2.10×10^5	29.19		mol/kg-atm	E
$HNO_3(g)$	$\Longleftrightarrow HNO_3(aq)$	2.10×10^5			mol/kg-atm	D
$HONO(g)$	$\Longleftrightarrow HONO(aq)$	4.90×10^1	16.04		mol/kg-atm	F
$HO_2NO_2(g)$	$\Longleftrightarrow HO_2NO_2(aq)$	2.00×10^4			mol/kg-atm	G
$N_2O(g)$	$\Longleftrightarrow N_2O(aq)$	2.50×10^{-2}			mol/kg-atm	M
$H_2S(g)$	$\Longleftrightarrow H_2S(aq)$	1.02×10^{-1}			mol/kg-atm	N
$SO_2(g)$	$\Longleftrightarrow SO_2(aq)$	1.22	10.55		mol/kg-atm	A
$H_2SO_4(g)$	$\Longleftrightarrow H_2SO_4(g)$	2.17×10^6	-31.92		mol/kg-atm	U
$CO(g)$	$\Longleftrightarrow CO(aq)$	9.55×10^{-4}			mol/kg-atm	N
$CO_2(g)$	$\Longleftrightarrow CO_2(aq)$	*			mol/kg-atm	T
$CH_4(g)$	$\Longleftrightarrow CH_4(aq)$	1.50×10^{-3}			mol/kg-atm	N
$HCHO(g)$	$\Longleftrightarrow HCHO(aq)$	3.46	8.19		mol/kg-atm	H
$HCOOH(g)$	$\Longleftrightarrow HCOOH(aq)$	5.39×10^3	18.9		mol/kg-atm	A
$CH_3OH(g)$	$\Longleftrightarrow CH_3OH(aq)$	2.20×10^2	16.44		mol/kg-atm	I
$CH_3O_2(g)$	$\Longleftrightarrow CH_3O_2(aq)$	6.00	18.79		mol/kg-atm	E
$CH_3OOH(g)$	$\Longleftrightarrow CH_3OOH(aq)$	2.27×10^2	18.82		mol/kg-atm	B
$C_2H_6(g)$	$\Longleftrightarrow C_2H_6(aq)$	2.00×10^{-3}			mol/kg-atm	N
$C_2H_4(g)$	$\Longleftrightarrow C_2H_4(aq)$	4.67×10^{-3}			mol/kg-atm	N
$C_2H_5OH(g)$	$\Longleftrightarrow C_2H_5OH(aq)$	2.12×10^2	16.44		mol/kg-atm	Q
$CH_3COOH(g)$	$\Longleftrightarrow CH_3COOH(aq)$	8.60×10^3	21.58		mol/kg-atm	A
$CH_3C(O)OOH(g)$	$\Longleftrightarrow CH_3C(O)OOH(aq)$	4.73×10^2	20.70		mol/kg-atm	B
$CH_3C(O)OONO_2(g)$	$\Longleftrightarrow CH_3C(O)OONO_2(aq)$	2.90	19.83		mol/kg-atm	J
$CH_3COCHO(g)$	$\Longleftrightarrow CH_3COCHO(aq)$	3.70×10^3	25.33		mol/kg-atm	K
$C_5H_8(g)$	$\Longleftrightarrow C_5H_8(aq)$	1.30×10^{-2}			mol/kg-atm	N
$C_6H_5CH_3(g)$	$\Longleftrightarrow C_6H_5CH_3(aq)$	0.15			mol/kg-atm	M
$HCl\ (g)$	$\Longleftrightarrow H^+ + Cl^-$	1.97×10^6	30.19	19.91	mol^2/kg^2-atm	A
Dissociation Reactions Used for Ocean Composition and Nonequilibrium Air-Ocean Transfer						
$HCHO(aq) + H_2O(aq)$	$\Longleftrightarrow H_2C(OH)_2(aq)$	1.82×10^3	13.49		—	L
$SO_2(aq) + H_2O(aq)$	$\Longleftrightarrow H^+ + HSO_3^-$	1.71×10^{-2}	7.04		mol/kg	A
$CO_2(aq) + H_2O(aq)$	$\Longleftrightarrow H^+ + HCO_3^-$	*			mol/kg	A
$NH_3(aq) + H^+$	$\Longleftrightarrow NH_4^+$	*			kg/mol	T
$HNO_3(aq)$	$\Longleftrightarrow H^+ + NO_3^-$	1.20×10^1	29.17	16.83	mol/kg	A
$HCl(aq)$	$\Longleftrightarrow H^+ + Cl^-$	1.72×10^6	23.15		mol/kg	O
$H_2O(aq)$	$\Longleftrightarrow H^+ + OH^-$	*			mol/kg	T
$H_2SO_4(aq)$	$\Longleftrightarrow H^+ + HSO_4^-$	1.00×10^3			mol/kg	R
$H_2O_2(aq)$	$\Longleftrightarrow H^+ + HO_2^-$	2.20×10^{-12}	-12.52		mol/kg	S
$HO_2(aq)$	$\Longleftrightarrow H^+ + O_2^-$	3.50×10^{-5}			mol/kg	R
$HONO(aq)$	$\Longleftrightarrow H^+ + NO_2^-$	5.10×10^{-4}	-4.23		mol/kg	F
$HCOOH(aq)$	$\Longleftrightarrow H^+ + HCOO^-$	1.86×10^{-4}	-0.05		mol/kg	A
$CH_3COOH(aq)$	$\Longleftrightarrow H^+ + CH_3COO^-$	1.75×10^{-5}	0.10		mol/kg	A
$B(OH)_3(aq)$	$\Longleftrightarrow H^+ + B(OH)_4^-$	*			mol/kg	T
$Si(OH)_4(aq)$	$\Longleftrightarrow H^+ + SiO(OH)_3^-$	*			mol/kg	T
$H_3PO_4(aq)$	$\Longleftrightarrow H^+ + H_2PO_4^-$	*			mol/kg	T
$HF(aq)$	$\Longleftrightarrow H^+ + F^-$	*			mol/kg	T
$H_2S(aq)$	$\Longleftrightarrow H^+ + HS^-$	*			mol/kg	T
HSO_3^-	$\Longleftrightarrow H^+ + SO_3^{2-}$	*			mol/kg	T
HCO_3^-	$\Longleftrightarrow H^+ + CO_3^{2-}$	*			mol/kg	T
$H_2PO_4^-$	$\Longleftrightarrow H^+ + HPO_4^{2-}$	*			mol/kg	T
HPO_4^{2-}	$\Longleftrightarrow H^+ + PO_4^{3-}$	*			mol/kg	T
$NH_4NO_3(s)$	$\Longleftrightarrow NH_4^+ + NO_3^-$	1.49×10^1	-10.40	17.56	mol^2/kg^2	A
$NH_4Cl(s)$	$\Longleftrightarrow NH_4^+ + Cl^-$	1.96×10^1	-6.13	16.92	mol^2/kg^2	A
$NH_4HSO_4(s)$	$\Longleftrightarrow NH_4^+ + HSO_4^-$	1.38×10^2	-2.87	15.83	mol^2/kg^2	A
$(NH_4)_2SO_4(s)$	$\Longleftrightarrow 2\ NH_4^+ + SO_4^{2-}$	1.82	-2.65	38.57	mol^3/kg^3	A
$NH_4HCO_3(s)$	$\Longleftrightarrow NH_4^+ + HCO_3^-$	1.08	-10.04		mol^2/kg^2	A
$NaNO_3(s)$	$\Longleftrightarrow Na^+ + NO_3^-$	1.20×10^1	-8.22	16.01	mol^2/kg^2	A
$NaCl(s)$	$\Longleftrightarrow Na^+ + Cl^-$	3.61×10^1	-1.61	16.90	mol^2/kg^2	A
$NaHSO_4(s)$	$\Longleftrightarrow Na^+ + HSO_4^-$	2.84×10^2	-1.91	14.75	mol^2/kg^2	A
$Na_2SO_4(s)$	$\Longleftrightarrow 2\ Na^+ + SO_4^{2-}$	4.80×10^{-1}	0.98	39.50	mol^3/kg^3	A
$NaHCO_3(s)$	$\Longleftrightarrow Na^+ + HCO_3^-$	3.91×10^{-1}	-7.54	-5.68	mol^2/kg^2	A
$Na_2CO_3(s)$	$\Longleftrightarrow 2Na^+ + CO_3^{2-}$	1.81×10^1	10.77	30.55	mol^3/kg^3	A
$KNO_3(s)$	$\Longleftrightarrow K^+ + NO_3^-$	8.72×10^{-1}	-14.07	19.39	mol^2/kg^2	A
$KCl(s)$	$\Longleftrightarrow K^+ + Cl^-$	8.68	-6.94	19.95	mol^2/kg^2	A
$KHSO_4(s)$	$\Longleftrightarrow K^+ + HSO_4^-$	2.40×10^1	-8.42	17.96	mol^2/kg^2	A

Table 1. (continued)

Reaction		A	B	C	Units	Reference
$K_2SO_4(s)$	$\Longleftrightarrow 2\,K^+ + SO_4^{2-}$	1.57×10^{-2}	-9.59	45.81	mol^3/kg^3	A
$KHCO_3(s)$	$\Longleftrightarrow K^+ + HCO_3^-$	1.40×10^1	-7.60	-2.52	mol^2/kg^2	A
$K_2CO_3(s)$	$\Longleftrightarrow 2K^+ + CO_3^{2-}$	2.54×10^5	12.46	36.73	mol^3/kg^3	A
$Mg(NO_3)_2(s)$	$\Longleftrightarrow Mg^{2+} + 2NO_3^-$	2.51×10^{15}			mol^3/kg^3	A
$MgCl_2$	$\Longleftrightarrow Mg^{2+} + 2Cl^-$	9.55×10^{21}			mol^3/kg^3	A
$MgSO_4(s)$	$\Longleftrightarrow Mg^{2+} + SO_4^{2-}$	1.08×10^5			mol^2/kg^2	A
$MgCO_3(s)$	$\Longleftrightarrow Mg^{2+} + CO_3^{2-}$	6.82×10^{-6}			mol^2/kg^2	A
$Ca(NO_3)_2(s)$	$\Longleftrightarrow Ca^{2+} + 2NO_3^-$	6.07×10^5			mol^3/kg^3	A
$CaCl_2(s)$	$\Longleftrightarrow Ca^{2+} + 2Cl^-$	7.97×10^{11}			mol^3/kg^3	A
$CaSO_4\text{-}2H_2O(s)$	$\Longleftrightarrow Ca^{2+} + SO_4^{2-} + 2H_2O(aq)$	4.32×10^{-5}			mol^2/kg^2	A
$CaCO_3(s)$ (calcite, aragonite)	$\Longleftrightarrow Ca^{2+} + CO_3^{2-}$	*			mol^2/kg^2	T

[a]References: A, *Jacobson* [1999a, Table B.6]; B, *Lind and Kok* [1986]; C, *Kozac-Channing and Heltz* [1983]; D, *Schwartz* [1984]; E, *Jacob* [1986]; F, *Schwartz and White* [1981]; G, *Park and Lee* [1987]; H, *Ledbury and Blair* [1925]; I, *Snider and Dawson* [1985]; J, *Lee* [1984]; K, *Betterton and Hoffmann* [1988]; L, *Le Henaff* [1968]; M, *Hoffmann and Calvert* [1985]; N, *Stumm and Morgan* [1981]; O, *Marsh and McElroy* [1985]; P, *Lide* [1998]; Q, *Wilson et al.* [2001]; R, *Perrin* [1982]; S, *Smith and Martell* [1976]; T, *Millero* [1995]; U, *Scott and Cattell* [1979]. The asterisk indicates a nonstandard temperature- and salinity- or ionic-strength dependent rate coefficient expression, given in the indicated reference, measured in seawater and that accounts for activity coefficients. The equilibrium coefficient reads, $K_{eq}(T) = A\,\exp\{B(\frac{T_0}{T}-1) + C(1-\frac{T_0}{T}+\ln\frac{T_0}{T})\}$, where $A = K_{eq}(T_0)$, $B = -\frac{1}{R^*T_0}\sum_i k_i\nu_i\Delta_f H_i^o$, $C = -\frac{1}{R^*}\sum_i k_i\nu_i c_{p,i}^o$, and $T_0 = 298.15$ K. The terms in A, B, and C are defined further in *Jacobson* [1999a, chapter 18].

is the ionic strength of seawater calculated here (mol kg^{-1}-dw) (where $z = +3, +2, +1, 0, -1, -2,$ or -3, is charge). From equation (11) the ratio of free hydrogen ions to total hydrogen is

$$\frac{m_{H^+}}{m_{H^+,SWS}} = \left[1 + \frac{m_{SO_4^{2-}}}{K_{HSO_4^-}^*} + \frac{m_{F^-}}{K_{HF}^*}\right]^{-1} \quad (15)$$

This ratio is necessary in equations (9) and (10) to ensure that the hydrogen ion molality in all terms in the model is that of free hydrogen.

[13] The salinity and density of seawater are calculated here as

$$S = 1000\left[\left(\sum c_q m_q\right) - c_{H_2O} m_{H_2O}\right] / \left(\sum c_q m_q\right) \quad (16)$$

$$\rho_{sw} = \frac{\rho_{dw}}{1 - 0.001S} \quad (17)$$

respectively, where the summation in the salinity equation is over all components in seawater, including dilute water, and m is molecular weight (g mol^{-1}). The ratio $\rho_{sw}/\rho_{dw} = 1/1 - 0.001S$) is necessary to convert reaction rate coefficients from mol kg^{-1}-sw to mol kg^{-1}-dw.

[14] For reactions in Table 1 for which seawater-measured rate coefficients were not available, the dilute-solution rate coefficients are given and activity coefficients of electrolytes in a mixture were calculated with the *Bromley* [1973] mixing rule, which requires temperature- and molality-dependent binary solute activity coefficient expressions. Expressions used for binary activity coefficients for electrolytes containing Na$^+$, Mg^{2+}, Ca^{2+}, K$^+$, NH$_4^+$, Cl$^-$, NO$_3^-$, HSO$_4^-$, and SO$_4^{2-}$, applicable to high ionic strength, are given in *Jacobson et al.* [1996], *Jacobson* [1999b], and *Lin and Tabazadeh* [2001]. For remaining electrolytes, which are present in only trace quantities, activity coefficients for individual ions in a mixture were calculated from the relatively simplistic Davies equation,

$$-\log_{10}\gamma_z = 0.5z^2\left(\frac{I^{1/2}}{1+I^{1/2}} - 0.2I\right)\left(\frac{298.15}{T_w}\right)^{2/3} \quad (18)$$

[e.g., *Butler*, 1982], where I is the ionic strength (mol kg^{-1}-dw) and T is absolute temperature (K). For a seawater ionic strength of $I = 0.716$ mol L^{-1} at 298.15 K, equation (18) predicts single-ion activity coefficients of univalent ions of $\gamma_{z=\pm1} = 0.69$ and of divalent ions of $\gamma_{z=\pm2} = 0.23$, which compares with experimental values between 0.63–0.71 for univalent ions and 0.26–0.28 for divalent ions, respectively [e.g., *Butler*, 1982, p. 121].

[15] The dry deposition speed in equation (1) is calculated as the inverse sum of a series of resistances [e.g., *Wesely and Hicks*, 1977; *Slinn et al.*, 1978; *Wesely*, 1989]. With the resistance model, the dry deposition speed of a gas is (m s^{-1}) is

$$V_{d,gas,q} = \frac{1}{R_{a,q} + R_{b,q} + R_{s,q}} \quad (19)$$

where $R_{a,q}$ is the aerodynamic resistance of the gas between a reference height (about 10 m above the surface) and the laminar sublayer adjacent to the surface, $R_{b,q}$ is the resistance to molecular diffusion through the 0.1 to 0.01-cm-thick laminar sublayer, and $R_{s,q}$ is the resistance to chemical, biological, and physical interaction and sticking between the surface and the gas once the gas has collided with the surface. *Jacobson* [1999a, chapter 20] gives expressions for the aerodynamic resistance and resistance to molecular diffusion used here.

[16] The resistance to surface interactions depends on properties of the surface and the depositing gas. The surface resistance over the ocean (s cm^{-1}) is calculated with

$$R_{s,q} = \frac{1}{\alpha_{r,q} H_q' k_{w,q}} \quad (20)$$

where H_q' is the dimensionless effective Henry's constant from equation (6), $\alpha_{r,q}$ is the dimensionless enhancement of gas transfer to sea water due to chemical reaction on the ocean surface, and $k_{w,q}$ is the transfer speed of a chemically unreactive gas through a thin film of water at the ocean

surface to the ocean mixed layer (cm s^{-1}). For extremely soluble gases, such as HCl, H_2SO_4, HNO_3, and NH_3, the dimensionless effective Henry's constant H'_q is large and $\alpha_{r,q}$ may be large, so the surface resistance ($R_{s,q}$) is small, and the dry deposition speed is limited only by the aerodynamic resistance ($R_{a,q}$) and the resistance to molecular diffusion ($R_{b,q}$). For slightly soluble gases, such as CO_2, CH_4, O_2, N_2, and N_2O, H'_q is relatively small, and $\alpha_{r,q} \approx 1$, so $R_{s,q}$ is large, and the dry deposition speed is controlled by $k_{w,q}$ [Liss and Merlivat, 1986].

[17] The transfer speed through a thin film of water on the ocean surface is affected by the gas' dissolution in and molecular diffusion through the film and surfactants and bursting of bubbles on the surface of the film. Although the transfer speed depends on several processes, parameterizations of $k_{w,q}$ to date have been derived only in terms of wind speed. The parameterization used here [Wanninkhof, 1992] is

$$k_{w,q} = \frac{0.31 \left| \mathbf{v}_{h,10} \right|^2}{3600} \left(\frac{\mathrm{Sc}_{w,CO_2,20^\circ C}}{\mathrm{Sc}_{w,q,T_{w,c}}} \right)^{1/2} \qquad (21)$$

where $k_{w,q}$ has units of cm s^{-1}, 3600 converts cm hr^{-1} to cm s^{-1}, $|\mathbf{v}_{h,10}|$ is the wind speed 10 m above sea level (m s^{-1}), $\mathrm{Sc}_{w,CO_2,20^\circ C}$ is the dimensionless Schmidt number of CO_2 in water at 20°C, and $\mathrm{Sc}_{w,q,T_{w,c}}$ is the Schmidt number of species q at current water temperature. An expression for the Schmidt number of CO_2 in seawater is

$$\mathrm{Sc}_{w,CO_2} = 2073.1 - 147.12 T_{w,c} + 3.6276 T_{w,c}^2 - 0.043219 T_{w,c}^3 \qquad (22)$$

[Wanninkhof, 1992], where $T_{s,c}$ is the temperature (°C) of seawater and the fit is valid for 0–30 °C. Another expression for the transfer speed is that of Liss and Merlivat [1986].

[18] Equation (1) gives the time-dependent change in gas mole concentration due to transfer to and from ocean water. Since the equation contains two unknowns, another equation is required to close it. The second equation is the air-ocean mass-balance equation,

$$c_{q,T,t} D_l + C_{q,t} \Delta z_a = c_{q,T,t-h} D_l + C_{q,t-h} \Delta z_a \qquad (23)$$

where D_l is the depth (cm) of the ocean mixed layer. Before equation (1) can be substituted, it must be rewritten by gathering $C_{q,t}$ terms on the left side and solving, giving

$$C_{q,t} = \frac{C_{q,t-h} + \frac{hV_{d,gas,q}}{\Delta z_a} \frac{c_{q,T,t}}{H'_q}}{1 + \frac{hV_{d,gas,q}}{\Delta z_a}} \qquad (24)$$

Substituting equation (24) into equation (23) and solving for the final ocean concentration at the end of a time step gives

$$c_{q,T,t} = \frac{c_{q,T,t-h} + \left[\frac{hV_{d,gas,q} C_{q,t-h}}{D_l} \middle/ \left(1 + \frac{hV_{d,gas,q}}{\Delta z_a} \right) \right]}{1 + \left[\frac{hV_{d,gas,q}}{D_l H'_q} \middle/ \left(1 + \frac{hV_{d,gas,q}}{\Delta z_a} \right) \right]} \qquad (25)$$

Equation (25) is then substituted back into equation (24) to give the final gas concentration for the time step. This solution (equations (24) and (25)), referred to as the Ocean Predictor for Dissolution (OPD), scheme, conserves mass exactly, is noniterative, and cannot produce a negative gas or ocean concentration, regardless of the time step. The equations can also be derived with exponential terms in a manner similar to that in Jacobson [1997] for the APD scheme, but the difference in accuracy is small.

3. Equilibrium Ocean Chemistry

[19] The OPD scheme solves ocean-atmosphere exchange of nondissociating/nonreacting or dissociating/reacting gases. When the scheme is used for transfer of a dissociating/reacting gas, an equilibrium solver is needed to calculate dissociation and reaction. The equilibrium solver determines the pH and concentrations of liquids, ions, and solids in the ocean.

[20] The equilibrium solver developed here is EQUISOLV O, which uses the solution mechanism of EQUISOLV II [Jacobson, 1999b], but with numerical changes described shortly and a different chemistry set. EQUISOLV O and EQUISOLV II solve any reactions listed in an input file, thus the equations are not wired in the code. The ocean reaction set (Table 1) differs from but has some overlap with the aerosol reaction set [Jacobson, 1999a, Table B.7]. For the current application, the equilibrium equations solved are all except those containing a gas in Table 1. The reactions in the table containing a gas are used to determine dimensionless effective Henry's constants (e.g., equation (6)) for gas transfer.

[21] EQUISOLV O solves equilibrium and activity coefficient equations, iterating over all equations until they converge. The water equation, used to determine the water content of aerosol particles, is not solved for the ocean since the ocean water content is only a trivial function of ocean composition. Within the iteration sequence among all equations, individual equilibrium equations must be solved. Three methods are used to solve individual equations. First, all equations with either 1 or 2 reactants and 1 or 2 products are solved analytically. Second, those with either 1 reactant and 3 products or vice-versa are solved with a Newton-Raphson solution that is guaranteed to converge due to the structure of the equation solved. The first two methods, together, are referred to as Analytical Equilibrium Iteration (AEI) methods [Jacobson, 1999b]. Finally, equations with five or more products plus reactants are solved with a mass-flux iteration technique (MFI) [Jacobson et al., 1996]. All three techniques are positive-definite and mass- and charge-conserving under all conditions. All equations in Table 1 are solved analytically with the first technique, so no iterations are required for any individual equation solved here.

[22] Because the solution to individual equations conserves mass- and charge and is positive-definite, the solution to all equations, following iteration around them also conserves mass- and charge and is positive for any number of iterations or equations, so long as the system is initialized in mass and charge balance. Other equilibrium solution methods include an iterative Newton-Raphson method, iterative bisectional Newton method, or iterative method

that minimized the Gibbs free energy. None of these methods guarantees a positive solution if iterations stop before convergence. Also, because such methods require first guesses, none is guaranteed to converge to positive roots (although most do for most calculations), and non-convergence occurs more frequently as the number of equations or grid cells increases, a characteristic found in practice [e.g., *Zhang*, 2000, section 3.2.3]. EQUISOLV O permits a positive-definite, mass-conserving, convergent solution to thousands of equations simultaneously, as demonstrated with the atmospheric version of the code in *Jacobson et al.* [1996, Figure 3 – 1400 equations] and *Fridlind et al.* [2000, section 3.1 – 2500 equations].

[23] Two improvements were made to EQUISOLV O. First, initial charge balance is now obtained by balancing the charge difference among all initial ions with both H^+ and OH- simultaneously. In EQUISOLV II, initial charge balance was obtained by adding $H+$ when the sum of all initial charges except H^+ was negative and adding carbonate or removing ammonium when the sum was positive. The initial mole concentrations of H^+ and $OH-$ are now found by solving the water dissociation equilibrium relation,

$$\rho_{dw}^2 K_w = \rho_{dw}^2 \mathbf{m}_{H^+} \mathbf{m}_{OH^-} = c_{H^+} c_{OH^-} \qquad (26)$$

for the reaction, $H_2O(aq) \iff H^+ + OH^-$, simultaneously with the charge-balance equation,

$$c_{H^+} + \sum_{q=1}^{N_I} z c_q = c_{OH^-} \qquad (27)$$

where K_w the equilibrium coefficient of the reaction $H_2O(aq) \iff H^+ + OH^-$ in seawater,

$$\ln K_w \left(\frac{mol^2}{kg^2 - dw} \right) =$$
$$\cdot \frac{\rho_{sw}}{\rho_{dw}} \left\{ \begin{array}{l} 148.9802 - \dfrac{13,847.26}{T_w} - 23.6521 \ln T_w \\[2mm] + \left(-5.977 + \dfrac{118.67}{T_w} + 1.0495 \ln T_w \right) S^{0.5} - 0.01615 S \end{array} \right\}$$
$$(28)$$

[*Millero*, 1995]. Also, N_I is the number of ions, excluding H^+ and OH^-, in sea water, and $z(=\pm1,2,3)$ is the charge of each ion. The exact solution to equations (26) and (27) is

$$c_{H^+} = -\frac{1}{2} \sum_{q=1}^{N_I} z c_q + \frac{1}{2} \sqrt{ \left(\sum_{q=1}^{N_I} z c_q \right)^2 + 4\rho_{dw}^2 K_w }$$
$$c_{OH^-} = \rho_{dw}^2 K_w / c_{H^+} \qquad (29)$$

The use of equation (29) allows initial charge to be balanced exactly and the water dissociation equation to be satisfied initially.

[24] Second, during iteration among all equations, the water dissociation equilibrium equation is now solved analytically for H^+ and OH^- simultaneously using equation (29). In *Jacobson* [1999b], no analytical solution for the water equation was derived, so when the equation was solved,

it was solved with the MFI technique, which requires iteration.

4. Results

[25] The schemes developed were analyzed in a two-box atmosphere-ocean model, a one-dimensional atmosphere-ocean model, and a three-dimensional global model.

4.1. Analysis of Equilibrium Ocean Composition

[26] The first analysis was to calculate ocean composition assuming equilibrium with the atmosphere, and to determine the sensitivity of composition to different chemicals and conditions. Transport and biology in the ocean were ignored. For this analysis, the model was run with one atmospheric compartment (box) and one ocean box. The atmospheric box was initialized (for the base case) with 375 ppmv CO_2. The atmosphere and ocean temperatures were initialized at 289.25 K, which is the globally averaged surface-ocean temperature from 1880–2003 [*National Climatic Data Center* (*NCDC*), 2004]. The mixing ratios of other gases were not relevant to the first simulation. To translate mixing ratio into globally averaged atmospheric mole concentration of CO_2, it was necessary to calculate the dry-air density in an atmospheric box that contains the global column abundance of air at constant density and temperature. Dry-air density (g cm^{-3}) was calculated as

$$\rho_d = \frac{p_s}{R' T} \qquad (30)$$

where R' is the gas constant for dry air (2870437.755 cm^2 s^{-2} K^{-1}), T is absolute air temperature (K), and p_s is the globally averaged dry-air surface pressure (g cm^{-1} s^{-2}),

$$p_s = \frac{N_T g m_d}{A 4 \pi R_e^2} \qquad (31)$$

where $N_T = 1.096 \times 10^{44}$ is the total number of nonwater vapor molecules in the air (calculated from a global model), g is gravity (980.6 cm s^{-2}), $m_d = 28.966$ g mol^{-1} is the molecular weight of dry air, $A = 6.0221367 \times 10^{23}$ g mol^{-1} is Avogadro's number, and $R_e = 637099700$ cm is the Earth's radius. The height (cm) of the atmospheric box is then

$$H = \frac{p_s}{g \rho_d} \qquad (32)$$

For example, for $T = 289.25$ K, air density, air pressure, and box height are 0.0012206585385 g cm^{-3}, 1013.4811945256 hPa, and 846700.1025 cm, respectively. Finally, the mole concentration (mol cm^{-3}) of any gas q in this box is

$$C_q = \chi_q \rho_d A / m_d \qquad (33)$$

where χ_q is the volume mixing ratio (number of molecules of a gas per molecule of dry air) of the gas, expressed as a fraction.

[27] Ocean composition for the base case was calculated assuming an initial ocean speciation given in Table 2 and

Table 2. Initial Near-Surface Concentrations of Major Seawater Constituents[a]

Constituent	Concentration, mg/L	Constituent	Concentration, mg/L
Na	10,800	Br	67.3
Mg	1290	F	1.3
Ca	412	N	0.5
K	399	C	28
Sr	7.9	B	4.44
Li	0.18	Si	2.2
Cl	19,400	P	0.06
S	905		

[a]From *Lide* [1998].

equilibrium with 375 ppmv $CO_2(g)$. The inorganic carbon content in the ocean was calculated, so the value in Table 2 was not used. The ocean equilibrium reactions included CO_2 dissolution and all the dissociation reactions in Table 1 affecting the species in Table 3. Calcite and aragonite were assumed not to form since dissolved calcium carbonate in the surface ocean is supersaturated with respect to calcite and aragonite, partly because magnesium poisons the surface of a growing calcite crystal, creating a magnesium-calcite crystal that is more soluble than calcite alone [e.g., *Stumm and Morgan*, 1981; *Butler*, 1982]. In deep water, calcium carbonate is usually undersaturated because its solubility increases with increasing pressure. At least one model has examined the calcite cycle over a period of thousands of years [*Archer and Maier-Reimer*, 1994]. Here, only a sensitivity test of the effect of calcite formation on ocean composition is discussed (Table 3).

[28] Table 3 shows results from the base and several sensitivity cases of ocean equilibrium. The base-case (second column) globally averaged near-surface equilibrium pH of the ocean at 375 ppmv CO_2 was 8.136; salinity was $S = 34.08$ ppth (equation (16)); seawater density was $\rho_{sw} = 1.034$ (equation (17)); and the inorganic carbon content was $C_T = 2.030$ mmol/kg. The carbonate alkalinity, defined as

$$A_c = \mathbf{m}_{HCO_3^-} + 2\mathbf{m}_{CO_3^{2-}} + \mathbf{m}_{OH^-} - \mathbf{m}_{H^+} \qquad (34)$$

was 2.198 mmol/kg. The values for these parameters are well within the range of measured values [e.g., *Stumm and Morgan*, 1981; *Butler*, 1982].

[29] The third column of Table 3 shows the sensitivity of the base-case results to borate, phosphate, and silicate. For this calculation, species containing B, P, or Si were not allowed to form. The removal of these species at a constant partial pressure of CO_2 increased pH by only 0.02 pH units but increased the dissolved inorganic carbon content by about 4.2 percent and carbonate alkalinity by about 4.6 percent.

[30] The fourth column of Table 3 shows the sensitivity of the base case to strontium (Sr), lithium (Li), bromine (Br), fluorine (F), and nitrogen (N), in addition to B, P, and Si. The new ions removed affected primarily charge balance (although HF(aq)/F$^-$ equilibrium was also considered). Removing Sr, Li, Br, F, N, B, P, and Si together increased pH and dissolved inorganic carbon by about 0.12 pH unit and 36.6 percent, respectively. The effect was stronger than removing only B, P, and Si. Most of the effect was due to

Br, whose concentration in Table 2 is much larger than that of Br, Li, F, or N.

[31] The fifth column of Table 3 shows the sensitivity of the base case to allowing calcite (which has a lower solubility product than aragonite in seawater) to precipitate. Calcite precipitation was modeled to have a large effect, decreasing the pH and the dissolved carbon content by 0.3 pH units and 21.5 percent, respectively. Calcite forms from the reaction, $Ca^{2+} + CO_3^{2-} \iff CaCO_3(s)$. As it forms, it removes the positively charged calcium ion, increasing H$^+$ to balance charge, lowering the pH. Although calcium formation also reduces the carbonate ion, much of the carbonate ion is replaced by gas-phase dissolution (at a constant CO_2 mixing ratio in this case), but the carbonate ion is not completely replaced because, in equilibrium the pH is lower, and the fraction of total inorganic carbon partitioning to carbonate decreases with decreasing pH.

[32] The sixth and seventh columns of Table 3 show the sensitivity of the base case to temperatures of 273.15 K and 298.15 K, respectively, instead of 288.15 K. At 273.15 K, dissolved inorganic carbon increased by about 6.7 percent (since the solubility of CO_2 in water increases with decreasing temperature) and pH dropped by about 0.06 pH units (due to the higher dissociated carbon content of the ocean) in comparison with the base case. At 288.15 K, dissolved inorganic carbon decreased and pH increased relative to the base case.

[33] Columns eight and nine of Table 3 show the sensitivity of the base case to 750 ppmv CO_2 (doubling) and 275 ppmv CO_2 (preindustrial), respectively, instead of 375 ppmv. The equilibrium pHs at 275 and 750 ppmv were 8.247 and 7.876, respectively, compared with 8.136 at 375 ppmv. Thus, a CO_2 doubling (375 to 750 ppmv) increased the hydrogen ion content by a factor of about 2.35 relative to preindustrial times.

4.2. Analysis of Numerical Stability and Conservation

[34] The OPD-EQUISOLV O scheme was next analyzed for numerical stability and conservation properties. For the analysis, the model was run with one atmospheric compartment (equations (30)–(33)) and one ocean compartment 100 m deep. The atmospheric box was initialized with 375 ppmv CO_2, 1.8 ppmv CH_4, and the mixing ratios of other gases, as given in Table 4. The ocean and atmospheric temperatures for the simulations were both 289.25 K, and the wind speed was 3 m/s. The ocean compartment was first initialized with the bulk composition data from Table 2. The ocean was then equilibrated with 375 ppmv of atmospheric CO_2 at the initial temperature to determine the initial ocean composition of all ions. For the initialization, the aqueous molalities of dissolved gases other than HCl, HNO$_3$, and CO_2, were initialized to zero (the chloride ion and nitrate ion concentrations were initialized from the Cl and N concentrations in Table 2, and the carbonate, bicarbonate, and dissolved carbon dioxide concentrations were calculated from equilibrium). Following initialization, atmospheric CO_2 was instantaneously doubled to 750 ppmv without instantaneous equilibration of the ocean.

[35] Nonequilibrium ocean-atmosphere exchange coupled with ocean equilibrium were simulated for 100 years using five different time steps between 6 hours and 1 year. The transfer speed was determined from equation (21). Figure 1a

Table 3. Base Case and Sensitivity Calculations of Ocean Composition Assuming Equilibrium Between the Ocean and Atmospheric CO_2[a]

(1) Chemical	(2) Base CO_2 375 ppmv $T = 289.25$ K, Mmol/kg	(3) Base, but no B, P, Si, Mmol/kg	(4) Base, but no B, P, Si, Sr, Li, Br, F, N, Mmol/kg	(5) Base, but With $CaCO_3(s)$, Mmol/kg	(6) Base, but at $T = 273.15$ K, Mmol/kg	(7) Base, but at $T = 298.15$ K, Mmol/kg	(8) Base, but 750 ppmv CO_2, Mmol/kg	(9) Base, but 275 ppmv CO_2, Mmol/kg
Cl^-	547.795	547.795	547.795	547.795	547.296	548.828	547.795	547.795
HSO_4^-	1.4450×10^{-6}	1.3904×10^{-6}	1.0469×10^{-6}	2.8805×10^{-6}	8.2320×10^{-7}	1.9415×10^{-6}	2.6313×10^{-6}	1.1205×10^{-6}
SO_4^{2-}	28.253	28.253	28.253	28.253	28.228	28.307	28.253	28.253
$CO_2(aq)$	0.013663	0.013663	0.013663	0.013663	0.023710	0.0106996	0.027326	0.010020
HCO_3^-	1.8388	1.91103	2.5381	0.92242	2.0500	1.7087	2.0195	1.7389
CO_3^{2-}	0.17753	0.19174	0.33829	0.044673	0.092466	0.23002	0.10707	0.21649
Br^-	0.84316	0.84316	0	0.84316	0.84240	0.84475	0.84316	0.84316
$B(OH)_3(aq)$	0.33689	0	0	0.37782	0.37451	0.31504	0.37350	0.31695
$B(OH)_4^-$	0.093567	0	0	0.052639	0.055560	0.11624	0.056963	0.11352
$Si(OH)_4(aq)$	0.075306	0	0	0.076824	0.077056	0.073999	0.076677	0.074451
$SiO(OH)_3^-$	0.0031106	0	0	0.0015919	0.0012890	0.0045647	0.0017392	0.0039657
$HF(aq)$	1.7624×10^{-7}	1.6958×10^{-7}	0	3.5132×10^{-7}	1.47087×10^{-7}	1.9962×10^{-7}	3.2093×10^{-7}	1.3666×10^{-7}
F^-	0.068500	0.068500	0	0.068500	0.068438	0.068629	0.06850	0.06850
NO_3^-	0.035735	0.035735	0	0.035735	0.035703	0.035803	0.035735	0.035735
$H_3PO_4(aq)$	3.554×10^{-12}	0	0	1.4981×10^{-11}	7.6164×10^{-12}	2.6351×10^{-12}	1.244×10^{-11}	2.0637×10^{-12}
$H_2PO_4^-$	0.000012668	0	0	0.000026785	0.000023330	0.000009529	0.000024341	0.000009486
HPO_4^{2-}	0.0016786	0	0	0.0017805	0.0018211	0.0015527	0.0017712	0.0016209
PO_4^{3-}	0.00024795	0	0	0.00013193	0.000093011	0.00038053	0.00014367	0.00030877
OH^-	0.0037571	0.0039047	0.005186	0.0018847	0.00060809	0.0089491	0.0020632	0.0048451
Na^+	470.278	470.278	470.278	470.278	469.849	471.165	470.278	470.278
Mg^{2+}	53.132	53.132	53.132	53.132	53.084	53.233	53.132	53.132
Ca^{2+}	10.291	10.291	10.291	10.291	10.282	10.310	10.291	10.291
K^+	10.216	10.216	10.216	10.216	10.207	10.235	10.216	10.216
Sr^{2+}	0.09026	0.09026	0	0.09026	0.090177	0.09043	0.09026	0.09026
Li^+	0.02596	0.02596	0	0.02596	0.02594	0.02601	0.02596	0.02596
H^+	7.3035×10^{-6}	7.0275×10^{-6}	5.2902×10^{-6}	1.4559×10^{-5}	8.4361×10^{-6}	7.0072×10^{-6}	1.3230×10^{-5}	5.6636×10^{-6}
$CaCO_3(s)$	0	0	0	0.61328	0	0	0	0
C_T	2.03001	2.11643	2.89004	1.59404	2.16616	1.9494	2.15392	1.96544
pH	8.13647	8.15320	8.27653	7.83686	8.07386	8.15446	7.87615	8.24691
A_c	2.19762	2.29841	3.21985	1.01364	2.23552	2.17769	2.23571	2.17675
I	699.495	699.507	699.627	697.522	698.772	700.866	699.424	699.534
S, ppth	34.0848	34.0562	34.0338	34.0589	34.0619	34.1425	34.0911	34.0815
ρ_{sw}, g/cm^3	1.03418	1.03415	1.03412	1.03415	1.03510	1.03229	1.03418	1.03417
ρ_{dw}, g/cm^3	0.99893	0.99893	0.99893	0.99893	0.99984	0.99705	0.99893	0.99893

[a]The simulations are discussed in the text. Major base-case conditions include ocean water and air temperature equal to 289.25 K, $CO_2 = 375$ ppmv, and no calcium carbonate formation permitted. In the table, C_T is total dissolved inorganic carbon [$H_2CO_3(aq) + HCO_3^- + CO_3^{2-}$]. The temperatures in columns 2, 6, and 7 are air and ocean temperatures.

**Table 4.** Initial Mixing Ratios of Gases in Most Simulations

Gas	Mixing Ratio, ppmv	Gas	Mixing Ratio, ppmv
$O_3(g)$	40 ppbv	$HNO_3(g)$	500 pptv
$H_2(g)$	530 ppbv	$HO_2NO_2(g)$	10 pptv
$H_2O_2(g)$	3 ppbv	$N_2O(g)$	311 ppbv
$NH_3(g)$	100 pptv	$SO_2(g)$	1 pptv
$HCl(g)$	90 pptv	$CO(g)$	110 ppbv
$NO(g)$	5 pptv	$CO_2(g)$	375 ppmv
$NO_2(g)$	40 pptv	$CH_4(g)$	1.8 ppmv

shows the modeled time-dependent molality of dissolved methane calculated with the noniterative OPD scheme for the different time steps. Since atmospheric chemistry and ocean biology were ignored and methane did not dissociate in solution, methane was affected by dissolution only. As such, this test was useful for examining the effect of time step size on the stability properties of the OPD scheme alone. Regardless of the step size, the OPD scheme gave the exact solution in the first time step of calculation. The scheme conserved mass exactly between the atmosphere and ocean, was nonoscillatory, and positive-definite at all time steps.

[36] Figures 1b and 1c show time-dependent changes in CO_2 and surface-ocean pH, respectively, obtained for different time steps over 100 years following a sudden doubling of CO_2. CO_2 and pH converged to the same value, regardless of the time step. The different pathways to convergence occurred because feedbacks varied with time step size. For example, the quantity of CO_2 dissolved during a time step depended on the pH at the beginning of the step. During long time steps, the amount of CO_2 dissolved undershot or overshot the correct value since the pH used for the calculation (at the beginning) was not the final pH. During subsequent time steps, both pH and dissolved carbon converged to their correct values. Oscillations are avoided for short time steps or when CO_2 is added gradually, rather than suddenly. For all time steps, the solutions in Figures 1b and 1c were unconditionally stable, positive-definite, and mass- and charge conserving.

[37] Figure 1d compares numerical stability of the OPD-EQUISOLV O scheme with the numerical instability of replacing the OPD scheme with an explicit forward-Euler calculation. For the simulation, the atmosphere was slightly unstably stratified and the wind speed about 8 m/s. Transfer of ammonia, nitric acid, and carbon dioxide were solved independently with the OPD scheme, but ocean chemistry in and diffusion through 38 ocean layers was solved simultaneously for all species following each ocean-air transfer calculation. The time step was 2.5 days. Figure 1d shows that, although the explicit scheme conserved mass, it caused ammonia and nitric acid mixing ratios to become negative after one time step and carbon dioxide to become numerically unstable after about 160 time steps. The OPD scheme produced mass-conserving, smooth, and positive-definite solution at the same noniterative time step and all longer time steps.
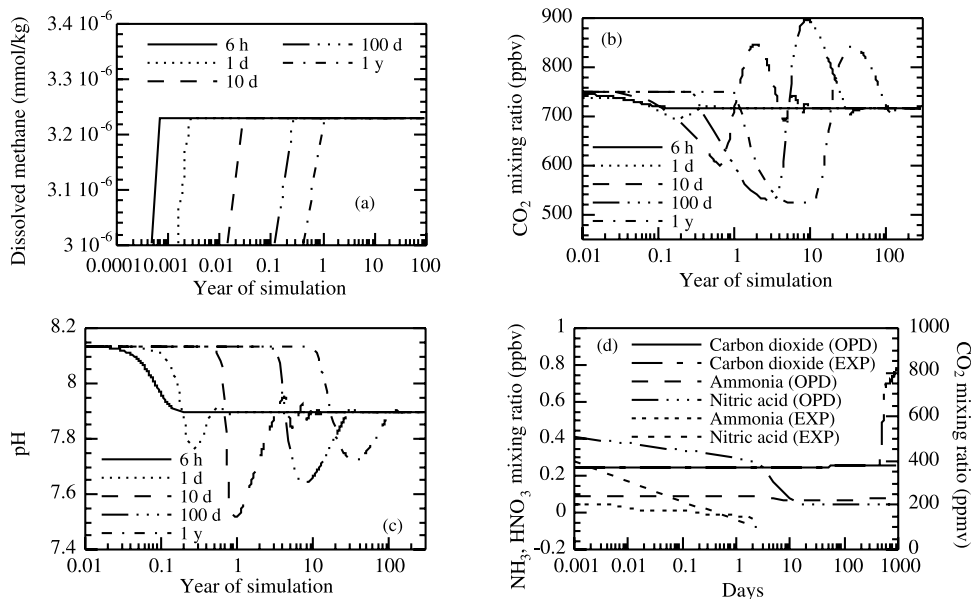
Figure 1. Modeled time-dependent molality of (a) dissolved CH_4, (b) atmospheric CO_2, and (c) ocean pH with the coupled OPD-EQUISOLV O scheme when the time step taken varied from six hours to one year, following an instantaneous doubling of CO_2 from 375 to 750 ppmv. Only one ocean and one atmospheric layer were treated. The ocean was initially equilibrated with the atmosphere at a CO_2 mixing ratio of 375 ppmv before CO_2 was doubled to 750 ppmv at the start of simulation. The temperature was 289.25 K, and the wind speed was 3 m/s. Initially, $CH_4(aq) = 0$ mmol/kg and $CH_4(g) = 1.8$ ppmv. (d) Comparison of modeled time-dependent atmospheric mixing ratios of ammonia, nitric acid, and carbon dioxide when the OPD-EQUISOLV O scheme was used ("OPD") with that when the OPD scheme was replaced by an explicit calculation ("EXP"), and the time step was 2.5 d. Only one time step of the explicit calculation is shown for ammonia and nitric acid since the solution is unrealistic following a negative value.
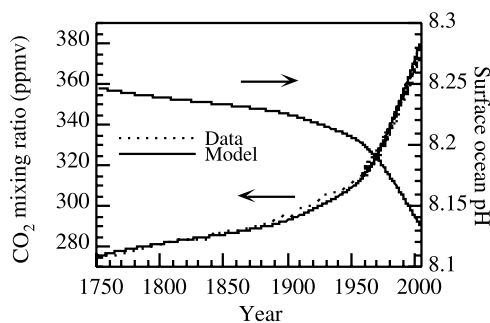
Figure 2. Modeled versus measured CO_2 mixing ratio and modeled surface ocean pH for 1750–2004 from a 1-D atmosphere-ocean calculation with OPD-EQUISOLV O. The model treated 38 ocean layers of 100-m thickness and one atmospheric layer divided into two compartments; land and ocean. CO_2 was emitted in the land compartment, partitioned each time step between the land-air and ocean-air compartment, and transferred between the ocean-air compartment and surface ocean. Dissolved CO_2 was diffused vertically in the ocean. Ocean chemistry was calculated in all layers. Other conditions for the simulation are described in the text. The CO_2 mixing ratio data were from *Friedli et al.* [1996] up to 1953 and from *Keeling and Whorf* [2003] for 1958–2003.

4.3. Examination of Historical and Future Atmosphere and Ocean Composition

[38] In this subsection, two applications are described. One is the calculation of CO_2 and ocean pH from 1751–2004 driven by an historic CO_2 emission inventory. The second is the calculation of CO_2 and pH from 2004 to 2104, driven by a future CO_2 emission scenario.

[39] In both cases, the model was extended to one dimension in the ocean and two compartments in the atmosphere. The ocean portion consisted of 38 100-m-thick layers (extending to a globally averaged ocean depth of 3800 m). The base-case initial ocean temperature and salinity profiles are given in Figure 3d. The surface ocean and atmospheric temperatures were set to 289.25 K (the globally averaged value sea-surface temperature from 1880 to 2003). Ocean and atmospheric temperatures were held constant during the base simulation.

[40] Each ocean layer was initialized by scaling the composition in Table 2 with the initial salinity profile in Figure 3d. For the historic case, each ocean layer was then equilibrated with a preindustrial CO_2 mixing ratio of 275 ppmv [e.g., *Friedli et al.*, 1996]. For the future case, each layer was initially equilibrated with a 2004 mixing ratio of 375 ppmv.

[41] For both cases, the atmosphere was divided into a land-air and ocean-air compartment. CO_2 was emitted into the land-air compartment. The added CO_2 was then instantaneously mixed between the ocean-air and land-air compartments, conserving mass, assuming the ocean comprises 71.3 percent of the Earth. Air-ocean exchange was then solved over the ocean. The ocean-air and land-air compartments were instantaneously mixed again following emission to land-air during the next time step.

[42] Historic fossil-fuel CO_2 emission data from 1751–2000 were taken from *Marland et al.* [2003]. A constant

emission rate of biomass burning from permanent deforestation of 500 Tg-C/yr from *Jacobson* [2004] (who estimates a range of 385–690 Tg-C/yr) was used, since biomass burning was not included in the fossil-fuel inventory. For the future case, the emission rate in 2000 was scaled to future years using the Special Report on Emission Scenarios (SRES) A1B CO_2 future emission scenario [*Nakicenovic et al.*, 2000], which is near the middle of future emission scenarios. Biomass-burning emission from permanent deforestation was assumed to stay at 500 Tg-C/yr for the future scenario.

[43] Base-case air-ocean exchange was calculated assuming a wind speed of 3 m/s. The calculated (constant) aerodynamic resistance and resistance to molecular diffusion for the base case were approximately 446 s m^{-1} and 317 s m^{-1}, respectively, which compare with a surface resistance of CO_2 (from equation (20)) at 289.25 K of near 2202 s m^{-1}. As such, dissolution controlled total CO_2 resistance.

[44] After each time step of air-ocean transfer, vertical diffusion was calculated in each ocean layer for each chemical. Diffusion was solved with an explicit, second-order, central difference scheme. For the diffusion coefficients used (1.5×10^{-4} to 1×10^{-5} m^2/s) and the time step size used (1 day), the scheme was unconditionally stable, mass-conserving, and positive definite for all species under all conditions. The canonical globally averaged deep-ocean diffusion coefficient is 1×10^{-4} m^2/s, but this value is a combination of smaller values (e.g., 1×10^{-5} m^2/s) over possibly 99 percent of the ocean and larger values (e.g., 1×10^{-2} m^2/s) over the remaining 1 percent [*Kantha and Clayson*, 2000, p. 679; *Kunze and Sanford*, 1996]. The larger values occur primarily near sloping topography and comprise most of the mixing. For the base case here, a value of 1×10^{-4} m^2/s was used in the upper deep ocean and a value of 1.5×10^{-4} m^2/s was used below that [*Jain et al.*, 1995], since the lower deep ocean is less stable than the upper deep ocean.

[45] Diffusion in the model was calculated by diffusing the difference from the initial vertical profile of each parameter, since the model did not treat biological processes or three-dimensional ocean transport, which are responsible for the vertical structure of carbon and salinity shown in Figures 3b and 3d, respectively. If the actual profile were diffused, the salinity and carbon gradients would disappear over time. When the difference from the initial condition is diffused, the gradients are maintained over time and additions to the gradients are diffused. Since biological feedbacks [e.g., *Sarmiento et al.*, 1992; *Maier-Reimer*, 1993b; *Klepper and De Haan*, 1995] depend on location-dependent parameters (e.g., nutrients and radiation), such feedbacks were not treated in the globally averaged one-dimension calculation here. Instead, the vertical carbon gradient was maintained during diffusion, as just described.

[46] Figure 2 shows modeled and measured $CO_2(g)$ and modeled surface-ocean pH from the historic 1751–2004 simulation. The simulation was run with a time step of one day. The model solved all the initialized gases in Table 4 and ocean chemicals in Table 3 (except that calcite/aragonite were assumed not to form). $CO_2(g)$ was neither nudged nor assimilated during the simulation; it was solved prognostically over time with the other variables. Considering

Table 5. Comparison of Some Results With Those From *Brewer* [1997] (B97)

Constituent	$CO_2(g)$-Model, ppmv	$CO_2(g)$-B97, ppmv	pH-Model	pH-B97	C_T-Model, mmol/kg	C_T-B97, mmol/kg
1751	275.0	—	8.247	—	1.965	—
1800	281.4	280	8.239	8.191	1.971	1.789
1996	365.0	360	8.148	8.101	2.026	1.869
2004	375.0	—	8.136	—	2.030	—
2084	750.0	—	7.876	—	2.154	—
2100	814.3	850	7.846	7.775	2.168	2.212

the simplifications made, the figure shows remarkable agreement of CO_2 with the historical CO_2 mixing ratio data of *Friedli et al.* [1996] (1744–1953) and *Keeling and Whorf* [2003] (1958–2003). As illustrated shortly with respect to the future scenarios, the agreement is sensitive to a much lower diffusion coefficient, a much lower wind speed, a large change in temperature (±3K) and a large reduction in permanent-deforestation biomass-burning emission. If the historic CO_2 results are indicative of the pH results, the figure suggests that ocean pH may have decreased from about 8.247 in 1751 to about 8.136 in 2004, for a 26 percent increase in the hydrogen ion content of the ocean. Table 5 compares pH and total carbon estimates for 1800 and 1996 to those from *Brewer* [1997], who used a two-compartment (ocean and atmosphere) model assuming equilibrium between the two and a specified partial pressure of CO_2 for different years. Despite significant differences in the model, the trends and magnitude of the results are similar. For example, *Brewer* [1997] calculated a decrease in pH of 0.09 pH units between 1800 and 1996; the reduction here was calculated as 0.091 pH units.
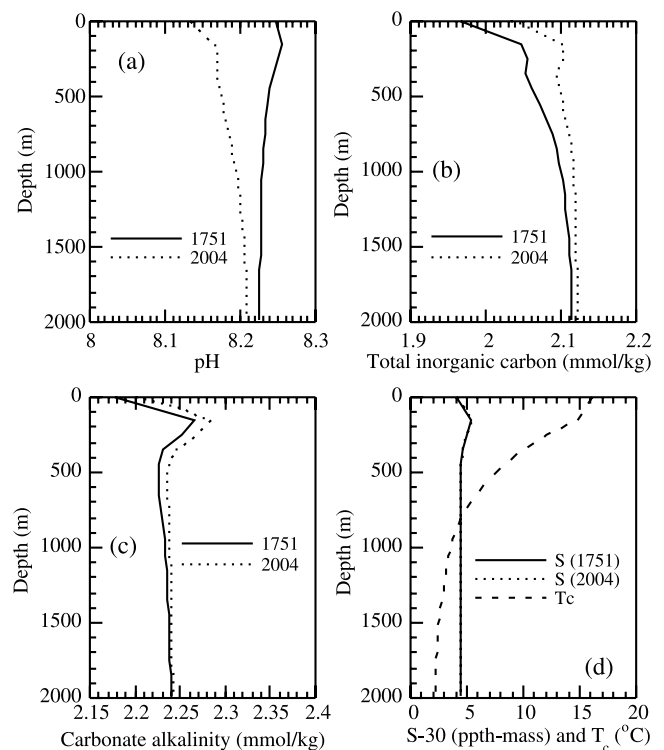
[47] Figure 3 shows modeled vertical profiles of several parameters in 1751 and 2004. Figure 3a shows that, as expected [e.g., *Caldeira and Wickett*, 2003], pH decreased from 1751–2004. The pH declined most near the surface. Similarly, the ocean inorganic carbon content and carbon alkalinity increased most near the surface. Salinity changed only slightly (Figure 3d) due to the relatively small change in ocean composition upon adding carbon. Temperatures (Figure 3d) were held constant during the simulation.

[48] Figure 4 shows results from the future A1B emission scenario for CO_2. The base case (wind speed of 3 m/s, temperature of 289.25 K, diffusion coefficient of 0.0001 m²/s, permanent deforestation biomass-burning emission of 500 Tg-C/yr) produced an estimated 814.3 ppmv of CO_2 and surface-ocean pH of 7.85 by 2100. Table 5 shows that the drop in modeled pH here between 1996 and 2000 was 0.302 pH units, whereas that estimated by *Brewer* [1997] was 0.326 although it should noted that *Brewer* [1997] specified a higher mixing ratio (850 ppmv) for 2100 versus the value calculated here under the A1B emission scenario of 814.3 ppmv. If the A1B emission scenario becomes reality and if the historic estimates here are correct, the hydrogen ion concentration in 2100 (pH = 7.846 from Table 5) may be a factor of 2.5 greater than in 1751 (pH = 8.247).

[49] Figure 4 shows the sensitivity of CO_2 and pH from the base case future scenario to several parameters. Figure 5 shows the corresponding sensitivities on dissolved inorganic carbon. Figure 4a shows that base-case CO_2 and ocean pH were sensitive to a lower wind speed (1 m/s) but not higher wind speed (5 m/s). At a lower wind speed, the transfer rate of CO_2 to the ocean was slowed considerably since the

transfer rate depended on the square of the wind speed (equation (21)). Because transfer occurred quite rapidly at 3 m/s (the base case), a faster wind speed had little further effect on the results.

[50] Figure 4b shows the sensitivity of future results to a 3 K lower and 3 K higher temperature than the base case. For the tests, the ocean was equilibrated initially with 375 ppmv CO_2 at the lower and higher temperature, respectively, so the initial pH differed from but the initial CO_2 was the same as that in the base case. A lower temperature decreased pH initially and in the end, as discussed with respect to the temperature sensitivity results in Table 3. The *Intergovernmental Panel on Climate Change* (*IPCC*) [2001] estimates that temperatures my increase by 1.4–5.8 K during the next 100 years. If correct, the 3 K higher case may be a more realistic sensitivity. In the 3-K higher case, less CO_2 was dissolved in the ocean during the initial equilibration, so the final dissolved carbon (Figure 5)

Figure 3. Modeled vertical profiles of (a) pH, (b) total carbon, (c) carbon alkalinity, and (d) salinity initially (1751), salinity at the end (2004), and temperature (the same for both dates) from the simulation described in the caption to Figure 2.
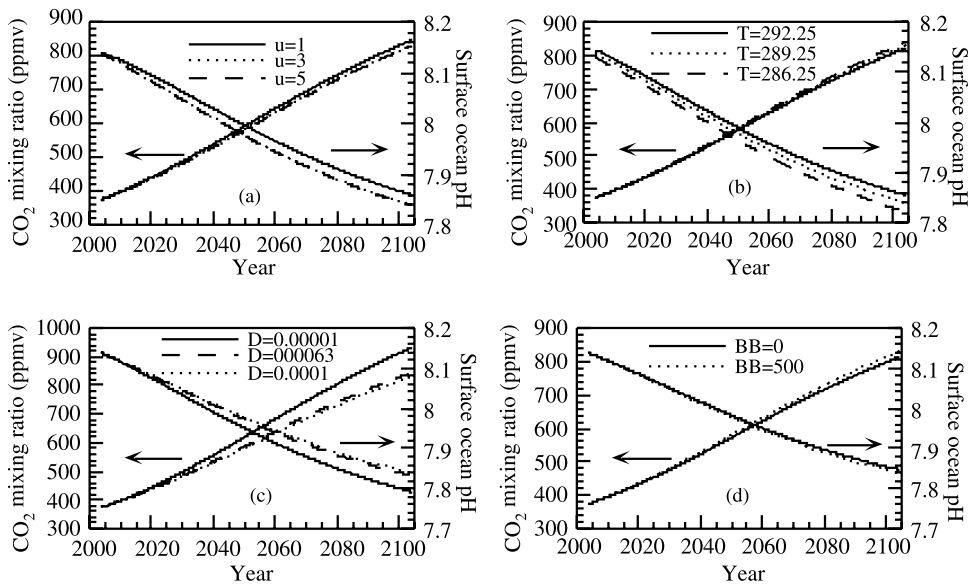
Figure 4. Modeled change in atmospheric CO_2 and surface-ocean pH between 2004 and 2104 under the conditions described in the caption to Figure 2, but using the Special Report on Emission Scenarios (SRES) A1B CO_2 future emission scenario [*Nakicenovic et al.*, 2000] and under different (a) wind speed (u, m/s), (b) water and atmospheric temperature (T, K), (c) ocean vertical diffusion coefficient (D, m^2/s), and (d) permanent-deforestation biomass burning emission (B, Tg-C/yr) estimates. The base case result (u = 3 m/s, T = 289.25 K, D = 0.0001 m^2/s, and B = 500 Tg-C/yr) is shown in each graph.

and CO_2 in the air (Figure 4b) were both lower and the ocean pH was higher than in the base case.

[51] Figure 4c shows that the base-case was sensitive to an ocean diffusion coefficient one-tenth that of the base value but much less so to one 40 percent lower than the base value. The very low diffusion case increased CO_2 because surface-ocean carbon could not dissipate to the deep ocean, suppressing transfer of CO_2 to the ocean. The higher ocean carbon near the surface also decreased pH near the surface relative to the base case. The 40-percent lower diffusion coefficient was sufficiently high to allow substantial diffusion of carbon to the deep ocean, resulting in relatively little difference between that case and the base case.

[52] Figure 4d shows that the base-case future result was slightly sensitive to the permanent-deforestation biomass-burning emission rate. The base-case permanent-deforestation biomass-burning emission rate (500 Tg-C/yr) was about 7.6 percent of the year 2000 emission rate of fossil-fuel CO_2 (6611 Tg-C/yr). Reducing the biomass burning emission rate to zero reduced CO_2 and increased pH in 2104 by about 18 ppmv and 0.1 pH units, respectively, relative to the base case.

[53] Figure 6 shows the initial (2004) and final (2104) vertical profiles of several parameters from the base future scenario. The results were qualitatively similar to those from Figure 3 for the historic scenario, but differed in magnitude due the greater expected increase in CO_2 during the next 100 years compared with during the last 250 years.

4.4. Effect of CO_2 on Other Acids and Bases

[54] Figure 7 illustrates the potential effect of an increase in CO_2 on the quantity of atmospheric acids and bases. Results from two sets of simulations are shown. Results for the first were obtained from the base-case future scenario

described in section 4.3, where the wind speed was 3 m/s and the atmosphere was neutrally stratified. Initial gas mixing ratios are given in Table 4. Ammonia and sulfur dioxide initially had no aqueous concentration. Hydrochloric acid and nitric acid were initially present in the ocean in the form of the chloride ion and the nitrate ion respectively (Table 2). No emission of these species was treated. Emission of CO_2 was treated in the base case. When ammonia transferred to the ocean from the atmosphere, its ocean concentration was controlled by $NH_3(aq) + H^+ \Longleftrightarrow NH_4^+$, which was affected by ocean pH. Dissolved sulfur dioxide was controlled by $SO_2(aq) \Longleftrightarrow H^+ + HSO_3^- \Longleftrightarrow 2H^+ + SO_3^{2-}$. Dissolved nitric acid was controlled by $HNO_3(aq) \Longleftrightarrow H^+ + NO_3^-$. Hydrochloric acid was assumed
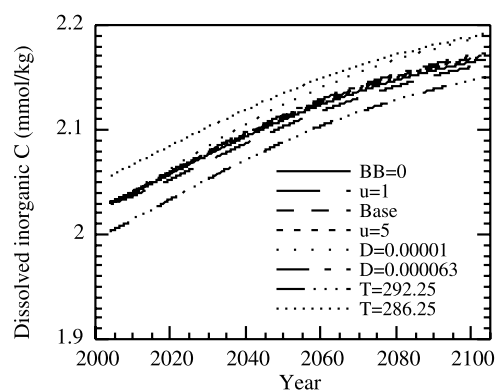
Figure 5. Total dissolved inorganic carbon in the surface-ocean layer between 2004 and 2104 ($H_2CO_3(aq) + HCO_3^- + CO_3^{2-}$) corresponding to each case shown in Figure 4.
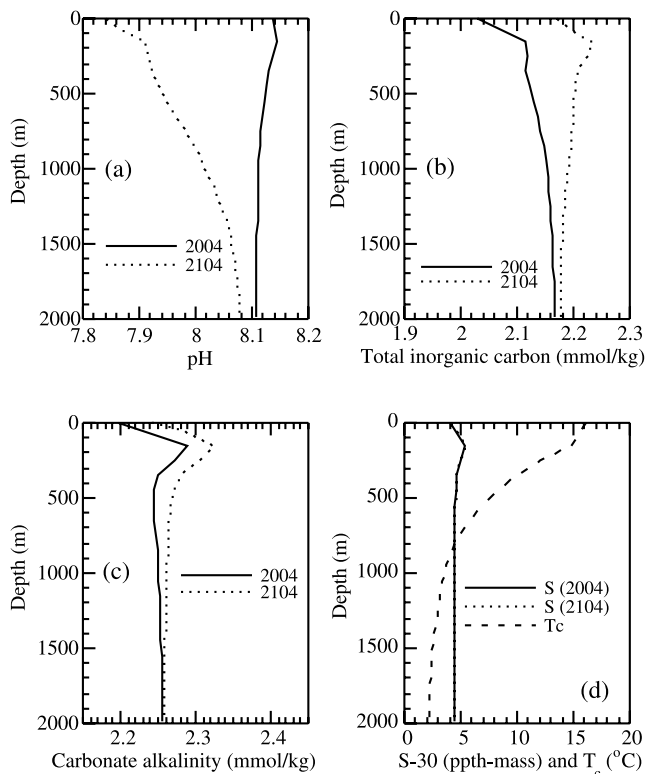
Figure 6. Modeled vertical profiles of (a) pH, (b) total carbon, (c) carbon alkalinity, and (d) salinity (S) and temperature (which was held constant for both dates) from the simulation described in the caption to Figure 4.

to dissociate completely. Rate coefficients for these reactions are given in Table 1.

[55] Figure 7a shows the time-dependent change in the mixing ratio of the four trace species from the base case. None of the gases was initially in equilibrium. The figure shows that the time to relative equilibrium was on the order of 5–10 years although complete equilibrium did not occur during the 100 years because mixing to the deep ocean was continuous. Figure 7b shows the result when the wind speed was 5 m/s. In that case, the time to relative equilibrium decreased to 3–8 years. When the wind speed was 1 m/s (not shown), the time to equilibrium increased to 10–25 years.

[56] Figure 7c shows the difference in the mixing ratios of the four species when future CO_2 emission was accounted for (the base case) minus when the CO_2 mixing ratio was held constant at 375 ppmv over time. The figure shows that an increase in CO_2 resulted in a slight increase in the transfer of acids (nitric, hydrochloric, and sulfurous) to the atmosphere and a larger transfer of the base ammonia from the atmosphere to the ocean. As CO_2 increased, it acidified the ocean, reducing the pH, increasing the ratio of $HNO_3(aq)/NO_3^-$, $SO2(aq)/HSO_3^-$, etc, and decreasing the ratio of $NH_3(aq)/NH_4^+$, forcing more acid to the air and more base to the water.

[57] Figure 7d shows results from a second set of simulations in which 58 Tg-NH_3 was continuously emitted globally and 25 percent of this was assumed to be present over the ocean. The figure shows NH_3 mixing ratios when
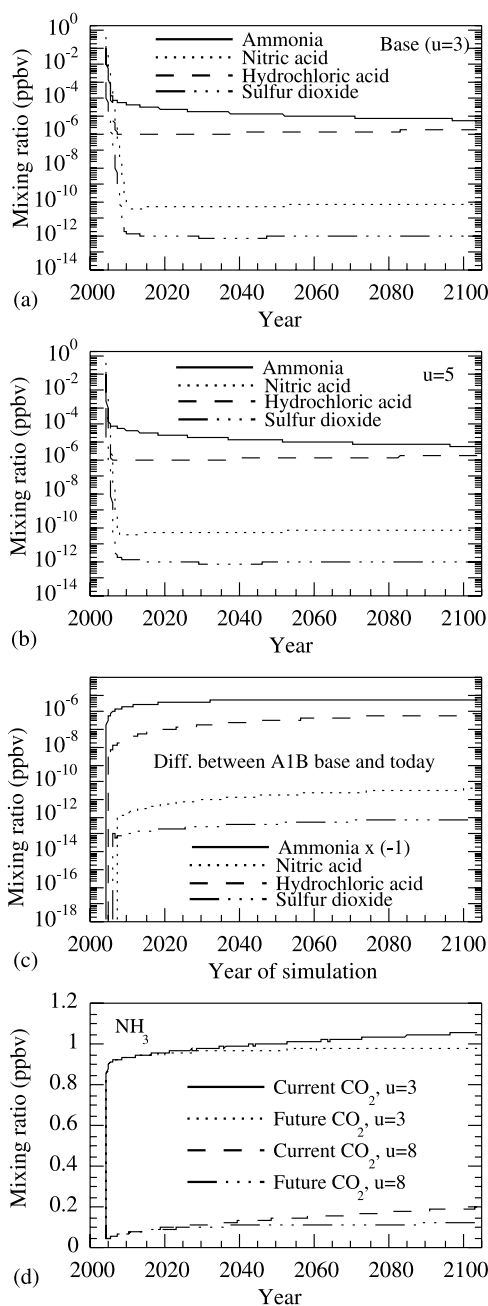
Figure 7. (a) Base-case (u = 3 m/s, T = 289.25 K, D = 0.0001 m²/s, B = 500 Tg-C/yr, and with SRES A1B fossil-fuel CO_2 emission but no emission of other species) change in gas-phase NH_3, HNO_3, HCl, and SO_2 from 2004 to 2104 found with the 1-D model and conditions used for Figure 4. (b) Same as Figure 7a, but when the wind speed was u = 5 m/s. (c) Difference between the base case and a case where CO_2 was held to 375 ppmv. (d) Change in NH_3 when its emission was treated and CO_2's emission was ("Future CO_2") or was not ("Current CO_2") treated and when different wind speeds were assumed. For u = 3 m/s, the atmosphere was neutral; for u = 8 m/s, it was slightly unstable.

CO_2 was held constant and when it changed according to the A1B emission scenario. Results suggest that the future decrease in ocean pH due to increasing CO_2 could result in a transfer of $7-40$ percent of ammonia over the ocean to the ocean. This would lead to a $0.015-0.02$ percent increase in the ammonium content of the ocean after 100 years.

[58] Simultaneous calculations suggest that decreasing ocean pH could increase the mixing ratio of HCl by about $0.001-0.003$ percent, of SO_2 by 0.0002 to 0.003 percent, and of HNO_3 by slightly less than of SO_2. These acids are affected less by a pH change than is ammonia because, at a high ocean pH, a reduction in pH has a greater effect on the $NH_3(aq)/NH_4^+$ ratio than on the $HNO_3(aq)/NO_3^-$, etc., ratio. A decrease in pH increases the atmospheric loading of weak acids to a greater degree than of strong acids.

[59] The changes in atmospheric ammonia and acids due to ocean acidification will slightly change the surface tension, vapor pressure, and activation properties of cloud condensation nuclei, resulting in a feedback to atmospheric radiation and climate.

4.5. Computer Timing in Three-Dimensional Global Ocean-Atmosphere Model

[60] The computer time of the code in the GATOR-GCMOM 3-D atmosphere-ocean model was tested. The time to solve ocean equilibrium among 22 reactions was 1.3676×10^{-6} s per iteration per grid cell per time step on a 3.2 GHz P4 Extreme processor. For a $4° \times 5°$ degree global grid with 2881 surface ocean grid cells, 10 layers (thus 28,810 total ocean cells), and 20 iterations per time step for convergence, the total computer time per time step was 0.9657 s. For a time step of 7200 s (2 hr), this translates to 1.17 hours per year of simulation. The computer time for noniterative nonequilibrium gas-ocean transfer of 90 gases with a 2-hr time step over the globe for the same year of simulation was about 20 s. In sum, the computer time to solve gas-ocean transfer and ocean equilibrium chemistry is relatively minor in comparison with that required for most other processes.

5. Conclusions

[61] A new numerical scheme, the Ocean Predictor of Dissolution (OPD) scheme, which solves nonequilibrium air-ocean transfer equations for any atmospheric constituent and time step, was developed. The scheme has several important properties: it is noniterative, implicit, mass-conserving, unconditionally stable, and positive-definite. When used alone to solve air-ocean exchange, it produces the exact solution without oscillation, regardless of the time step. A new chemical equilibrium module, EQUISOLV O, was also developed to solve chemical equilibrium in the ocean (and between the air and ocean when required), either independently or coupled with the nonequilibrium OPD scheme. EQUISOLV O converges iteratively, but is positive-definite and mass and charge conserving, regardless of the number of iterations taken. Two advances of EQUISOLV O over its atmospheric counterpart, EQUISOLV II, were the development of a new method to initialize charge and a noniterative solution to the water dissociation equation.

[62] The OPD-EQUISOLV O schemes were integrated into a 1-D-ocean/two-compartment atmospheric model driven by emission to examine the change in atmospheric CO_2 and ocean composition/pH between $1751-2004$ and $2004-2104$. CO_2 calculated from the historic simulation compared well with measured CO_2. Surface ocean pH was found to decrease from near 8.25 in 1751 to near 7.85 in 2100 under the combined historic emission record and future SRES A1B future emission scenario, resulting in a factor of 2.5 increase in ocean H^+ in 2100 relative to 1751.

[63] "Ocean acidification" due to CO_2 may also cause a nonnegligible transfer of the base ammonia from the atmosphere to the ocean and a smaller transfer of strong acids (e.g., hydrochloric, sulfurous, nitric) from the ocean to the atmosphere. Weak acids should be transferred to the atmosphere to a greater extent than strong acids. The existence and direction of these feedbacks are almost certain, suggesting that CO_2 buildup may have an additional impact on ecosystems. The time to relative equilibrium of atmospheric acids and bases with the full ocean may range from $3-8$ years with a moderately fast wind speed to $10-30$ years with a slow wind speed.

[64] The computer time of the OPD/EQUISOLV O scheme in the 3-D GATOR-GCMOM atmospheric model over a 4×5 degree horizontal grid with 10 layers of ocean was found to be less than two hours per year of simulation on a modern single processor.

References

Archer, D., and E. Maier-Reimer (1994), Effect of deep-sea sedimentary calcite preservation on atmospheric CO_2 concentration, *Nature*, *367*, 260–263.

Bassett, M. E., and J. H. Seinfeld (1983), Atmospheric equilibrium model of sulfate and nitrate aerosol, *Atmos. Environ.*, *17*, 2237–2252.

Betterton, E. A., and M. R. Hoffmann (1988), Henry's law constants of some environmentally important aldehydes, *Environ. Sci. Technol.*, *22*, 1415–1418.

Brewer, P. G. (1997), Ocean chemistry of the fossil fuel CO_2 signal: The haline signal of "business as usual," *Geophys. Res. Lett.*, *24*, 1367–1369.

Bromley, L. A. (1973), Thermodynamic properties of strong electrolytes in aqueous solutions, *AIChE J.*, *19*, 313–320.

Butler, J. N. (1982), *Carbon Dioxide Equilibria and Their Applications*, 259 pp., Addison-Wesley, Boston, Mass.

Byrne, R. H., Jr., and D. R. Kester (1974), Inorganic speciation of boron in seawater, *J. Mar. Res.*, *32*, 119–127.

Caldeira, K., and M. R. Rampino (1993), Aftermath of the end-cretaceous mass extinction: Possible biogeochemical stabilization of the carbon cycle and climate, *Paleoceanography*, *8*, 515–525.

Caldeira, K., and M. E. Wickett (2003), Anthropogenic carbon and ocean pH, *Nature*, *425*, 365.

Chang, W., B. G. Heikes, and M. Lee (2004), Ozone deposition to the sea surface: Chemical enhancement and wind speed dependence, *Atmos. Environ.*, *38*, 1053–1059.

Clegg, S. L., and M. Whitfield (1995), A chemical model of seawater including dissolved ammonia and the stoichiometric dissociation constant for ammonia in estuarine water and seawater from −2 to 40°C, *Geochim. Cosmochim. Acta*, *59*, 2403–2421.

Dickson, A. G. (1990), Standard potential of the reaction: AgCl(s) + $1.2H_2$(g) = Ag(s) + HCl(aq), and the standard acidity constant of the ion HSO_4^- in synthetic sea water from 273.15 to 318.15, *J. Chem. Thermodyn.*, *22*, 113–127.

Dickson, A. G., and F. J. Millero (1987), A comparison of the equilibrium constants for the dissociation of carbonic acid in seawater media, *Deep Sea Res.*, *34*, 1733–1743.

Dickson, A. G., and J. P. Riley (1979), The estimation of acid dissociation constants in seawater from potentiometric titrations with strong base. I. The ion product of water-K_w, Mar. Chem., 7, 89–99.

Dickson, A. G., and M. Whitfield (1981), An ion-association model for estimating acidity constants (at 25°C and 1 atm total pressure) in electrolyte mixtures related to seawater (ionic strength <1 mol kg^{-1} H$_2$O), Mar. Chem., 10, 315–333.

Fridlind, A. M., M. Z. Jacobson, V.-M. Kerminen, R. E. Hillamo, V. Ricard, and J.-L. Jaffrezo (2000), Analysis of gas-aerosol partitioning in the Arctic: Comparison of size-resolved equilibrium model results with field data, J. Geophys. Res., 105, 19,891–19,904.

Friedli, H., H. Lötscher, H. Oeschger, U. Siegenthaler, and B. Stauffer (1996), Ice core record of ^{13}C/^{12}C ratio of atmospheric CO$_2$ in the past two centuries, Nature, 324, 237–238.

Galbally, I. E., and C. R. Roy (1980), Destruction of ozone at the earth's surface, Q. J. R. Meteorol. Soc., 106, 599–620.

Garrels, R. M., and M. E. Thompson (1962), A chemical model for seawater at 25°C and one atmosphere total pressure, Am. J. Sci., 260, 57–66.

Goldberg, E. D., and G. O. S. Arrhenius (1958), Chemistry of Pacific pelagic sediments, Geochim. Cosmochim. Acta, 13, 153–212.

Goyet, C., and A. Poisson (1989), New determination of carbonic acid dissociation constants in seawater as a function of temperature and salinity, Deep Sea Res., 36, 1635–1654.

Greenberg, J. P., and N. Moller (1989), The prediction of mineral solubilities in natural waters: A chemical equilibrium model for the Na-K-Ca-Cl-SO$_4$-H$_2$O system to high concentration from 0 to 250°C, Geochim. Cosmochim. Acta, 53, 2503–2518.

Guggenheim, E. A. (1935), Thermodynamic properties of aqueous solutions of strong electrolytes, Philos. Mag., 19, 588–643.

Gurney, K. R., et al. (2002), Towards robust regional estimates of CO$_2$ sources and sinks using atmospheric transport models, Nature, 415, 626–630.

Hansson, I. (1973), A new set of acidity constants for carbonic acid and boric acid in sea water, Deep Sea Res., 20, 461–478.

Harvie, C. E., N. Moller, and J. H. Weare (1984), The prediction of mineral solubilities in natural waters: The Na-K-Mg-Ca-H-Cl-SO$_4$-OH-HCO$_3$-CO$_3$-CO$_2$-H$_2$O system to high ionic strengths at 25°C, Geochim. Cosmochim. Acta, 48, 723–751.

Hoffmann, M. R., and J. G. Calvert (1985), Chemical transformation modules for Eulerian acid deposition models, vol. 2, The aqueous-phase chemistry, EPA/600/3-85/017, U.S. Environ. Prot. Agency, Research Triangle Park, N. C.

Intergovernmental Panel on Climate Change (IPCC) (2001), Third Assessment Report, Climate Change 2001: The Scientific Basis, edited by J. T. Houghton et al., Cambridge Univ. Press, New York.

Jacob, D. J. (1986), Chemistry of OH in remote clouds and its role in the production of formic acid and peroxymonosulfonate, J. Geophys. Res., 91, 9807–9826.

Jacobson, M. Z. (1997), Numerical techniques to solve condensational and dissolutional growth equations when growth is coupled to reversible reactions, Aerosol Sci. Technol., 27, 491–498.

Jacobson, M. Z. (1999a), Fundamentals of Atmospheric Modeling, 656 pp., Cambridge Univ. Press, New York.

Jacobson, M. Z. (1999b), Studying the effects of calcium and magnesium on size-distributed nitrate and ammonium with EQUISOLV II, Atmos. Environ., 33, 3635–3649.

Jacobson, M. Z. (2002), Analysis of aerosol interactions with numerical techniques for solving coagulation, nucleation, condensation, dissolution, and reversible chemistry among multiple size distributions, J. Geophys. Res., 107(D19), 4366, doi:10.1029/2001JD002044.

Jacobson, M. Z. (2004), The short-term cooling and long-term global warming due to biomass burning, J. Clim., 17, 2909–2926.

Jacobson, M. Z., A. Tabazadeh, and R. P. Turco (1996), Simulating equilibrium within aerosols and nonequilibrium between gases and aerosols, J. Geophys. Res., 101, 9079–9091.

Jain, A. K., H. S. Kheshgi, M. I. Hoffert, and D. J. Wuebbles (1995), Distribution of radiocarbon as a test of global carbon cycle models, Global Biogeochem. Cycles, 9, 153–166.

Kantha, L. H., and C. A. Clayson (2000), Small Scale Processes in Geophysical Fluid Flows, Elsevier, New York.

Keeling, C. D., and T. P. Whorf (2003), Atmospheric CO$_2$ concentrations (ppmv) derived from in situ air samples collected at Mauna Loa Observatory, Hawaii, Oak Ridge Natl. Lab., Oak Ridge, Tenn.

Kell, G. S. (1972), Water and Aqueous Solutions, edited by R. A. Horne, p. 331, Wiley-Interscience, Hoboken, N. J.

Kettle, A. J., and M. O. Andreae (2000), Flux of dimethylsulfide from the oceans: A comparison of updated data sets and flux models, J. Geophys. Res., 105, 26,793–26,808.

Kim, Y. P., J. H. Seinfeld, and P. Saxena (1993), Atmospheric gas-aerosol equilibrium I. Thermodynamic model, Aerosol Sci. Technol., 19, 157–181.

Klepper, O., and B. J. De Haan (1995), A sensitivity study of the effect of global change on ocean carbon uptake, Tellus, Ser. B, 47, 490–500.

Kozac-Channing, L. F., and G. R. Heltz (1983), Solubility of ozone in aqueous solutions of 0–0.6 M ionic strength at 5–30°C, Environ. Sci. Technol., 17, 145–149.

Kunze, E., and T. B. Sanford (1996), Abyssal mixing: Where it is not, J. Phys. Oceanogr., 26, 2286–2296.

Ledbury, W., and E. W. Blair (1925), The partial formaldehyde vapour pressure of aqueous solutions of formaldehyde, II, J. Chem. Soc., 127, 2832–2839.

Lee, Y.-N. (1984), Kinetics of some aqueous-phase reactions of peroxyacetyl nitrate, in Gas-Liquid Chemistry of Natural Waters, vol. 1, BNL 51757, pp. 20/1–20/10, Brookhaven Natl. Lab., Upton, New York.

Le Henaff, P. (1968), Méthodes d'étude et propriétés des hydrates, hemiacétals et hemiacétals dérivés des aldéhydes et des cétones, Bull. Soc. Chim. France, 11, 4687–4700.

Leyendekkers, J. V. (1972), The chemical potential of seawater components, Mar. Chem., 1, 75–88.

Lide, D. R. (Ed.) (1998), CRC Handbook of Chemistry and Physics, CRC Press, Boca Raton, Fla.

Lin, J. S., and A. Tabazadeh (2001), An aerosol physical chemistry model for the NH$_3$/H$_2$SO$_4$/HNO$_3$/H$_2$O system at cold temperatures, J. Geophys. Res., 106, 4815–4829.

Lind, J. A., and G. L. Kok (1986), Henry's law determinations for aqueous solutions of hydrogen peroxide, methylhydroperoxide, and peroxyacetic acid, J. Geophys. Res., 91, 7889–7895.

Liss, P. S., and L. Merlivat (1986), Air-sea gas exchange rates: Introduction and synthesis, in The Role of Air-Sea Exchange in Geochemical Cycling, edited by P. Buat-Menard, pp. 113–127, Springer, New York.

Maier-Reimer, E. (1993a), Geochemical cycles in an ocean general circulation model: Preindustrial tracer distributions, Global Biogeochem. Cycles, 7, 645–677.

Maier-Reimer, E. (1993b), The biological pump in the fossil-fuel CO$_2$ uptake by the ocean, Global Planet. Change, 8, 13–15.

Maier-Reimer, E., and K. Hasselmann (1987), Transport and storage of CO$_2$ in the ocean, an inorganic ocean circulation carbon cycle model, Clim. Dyn., 2, 63–90.

Makar, P. A., V. S. Vouchet, and A. Nenes (2003), Inorganic chemistry calculations using HETV—A vectorized solver for the SO$_4^{2-}$-NO$_3^-$-NH$_4^+$ system based on the ISORROPIA algorithms, Atmos. Environ., 37, 2279–2294.

Marland, G., T. A. Boden, and R. J. Andres (2003), Global CO$_2$ emissions from fossil-fuel burning, cement manufacture, and gas flaring: 1751–2000, in Trends Online: A Compendium of Data on Global Change, Carbon Dioxide Inf. Anal. Cent., Oak Ridge Natl. Lab., U.S. Dep. of Energy, Oak Ridge, Tenn.

Marsh, A. R. W., and W. J. McElroy (1985), The dissociation constant and Henry's law constant of HCl in aqueous solution, Atmos. Environ., 19, 1075–1080.

Mehrbach, C., C. H. Culberson, J. E. Hawley, and R. M. Pytkowicz (1973), Measurement of the apparent dissociation constants of carbonic acid in seawater at atmospheric pressure, Limnol. Oceanogr., 18, 897–907.

Metzger, S., F. Dentener, S. Pandis, and J. Lelieveld (2002), Gas/aerosol partitioning: 1. A computationally efficient model, J. Geophys. Res., 107(D16), 4312, doi:10.1029/2001JD001102.

Millero, F. J. (1974), The physical chemistry of seawater, Ann. Rev. Earth Planet. Sci., 2, 101–150.

Millero, F. J. (1995), Thermodynamics of the carbon dioxide system in the oceans, Geochim. Cosmochim. Acta, 59, 661–667.

Millero, F. J., and D. J. Hawke (1992), Ionic interactions of divalent metals in natural waters, Mar. Chem., 40, 19–48.

Millero, F. J., and D. Pierrot (1998), A chemical equilibrium model for natural waters, Aquat. Chem., 4, 153–199.

Millero, F. J., and D. R. Schreiber (1982), Use of the ion pairing model to estimate activity coefficients of the ionic components of natural waters, Am. J. Sci., 282, 1508–1540.

Moller, N. (1988), The prediction of mineral solubilities in natural waters: A chemical equilibrium model for the Na-Ca-Cl-SO$_4$-H$_2$O system, to high temperature and concentration, Geochim. Cosmochim. Acta, 52, 821–837.

Murayama, S., S. Tagachi, and K. Higuchi (2004), Interannual variation in the atmospheric CO$_2$ growth rate: Role of atmospheric transport in the Northern Hemisphere, J. Geophys. Res., 109, D02305, doi:10.1029/2003JD003729.

Nakicenovic, N., et al. (2000), Emissions Scenarios: A Special Report of the Intergovernmental Panel on Climate Change, Cambridge Univ. Press, New York.

National Climatic Data Center (NCDC) (2004), Global long-term mean land and sea surface temperatures, Asheville, N. C.

Nenes, A., S. N. Pandis, and C. Pilinis (1998), ISORROPIA: A new thermodynamic equilibrium model for multiphase multicomponent inorganic aerosols, *Aquat. Geochem.*, *4*, 123–152.

Olsen, S. C., and J. T. Randerson (2004), Differences between surface and column atmospheric CO_2 and implications for carbon cycle research, *J. Geophys. Res.*, *109*, D02301, doi:10.1029/2003JD003968.

Pabalan, R. T., and K. S. Pitzer (1987), Thermodynamics of concentrated electrolyte mixtures and the prediction of mineral solubilities to high temperatures for mixtures in the system Na-K-Mg-Cl-SO_4-OH-H_2O, *Geochim. Cosmochim. Acta*, *51*, 2429–2443.

Park, J.-Y., and Y.-N. Lee (1987), Aqueous solubility and hydrolysis kinetics of peroxynitric acid, paper presented at 193rd Meeting, Am. Chem. Soc., Denver, Colo., 5–10 April.

Perrin, D. D. (1982), *Ionization Constants of Inorganic Acids and Bases in Aqueous Solution*, 2nd ed., Elsevier, New York.

Pilinis, C., and J. H. Seinfeld (1987), Continued development of a general equilibrium model for inorganic multicomponent atmospheric aerosols, *Atmos. Environ.*, *21*, 2453–2466.

Pitzer, K. S. (1973), Thermodynamics of electrolytes. I. Theoretical basis and general equations, *J. Phys. Chem.*, *77*, 268–277.

Pytkowicz, R. M. (1969), Use of apparent equilibrium constants in chemical oceanography, geochemistry, and biochemistry, *Geochim. J.*, *3*, 181–184.

Roy, R. N., L. N. Roy, K. M. Vogel, C. P. Moore, T. Pearson, C. E. Good, F. J. Millero, and D. M. Campbell (1993), Determination of the ionization constants of carbonic acid in seawater, *Mar. Chem.*, *44*, 249–268.

Sarmiento, J. L., J. C. Orr, and U. Siegenthaler (1992), A perturbation simulation of CO_2 uptake in a general circulation model, *J. Geophys. Res.*, *97*, 3621–3645.

Saxena, P., A. B. Hudischewskyj, C. Seigneur, and J. H. Seinfeld (1986), A comparative study of equilibrium approaches to the chemical characterization of secondary aerosols, *Atmos. Environ.*, *20*, 1471–1483.

Schwartz, S. E. (1984), Gas- and aqueous-phase chemistry of HO_2 in liquid water clouds, *J. Geophys. Res.*, *89*, 11,589–11,598.

Schwartz, S. E., and W. H. White (1981), Solubility equilibria of the nitrogen oxides and oxyacids in aqueous solution, *Adv. Environ. Sci. Eng.*, *4*, 1–45.

Scott, W. D., and F. C. R. Cattell (1979), Vapor pressure of ammonium sulfates, *Atmos. Environ.*, *13*, 307–317.

Sillen, L. G. (1961), The physical chemistry of seawater, in *Oceanography*, edited by M. Sears, *Am. Assoc. Adv. Sci. Publ.*, *67*, 549–581.

Slinn, W. G. N., L. Hasse, B. B. Hicks, A. W. Hogan, D. Lal, P. S. Liss, K. O. Munnich, G. A. Sehmel, and O. Vittori (1978), Some aspects of the transfer of atmospheric trace constituents past the air-sea interface, *Atmos. Environ.*, *12*, 2055–2087.

Smith, R. M., and A. E. Martell (1976), *Critical Stability Constants*, vol. 4, *Inorganic Complexes*, Springer, New York.

Snider, J. R., and G. A. Dawson (1985), Tropospheric light alcohols, carbonyls, and acetonitrile: Concentrations in the southwestern United States and Henry's law data, *J. Geophys. Res.*, *90*, 3797–3805.

Spencer, R. J., N. Moller, and J. H. Weare (1990), The prediction of mineral solubilities in natural waters: A chemical equilibrium model for the Na-K-Ca-Mg-Cl-SO_4-H_2O system at temperatures below 25°C, *Geochim. Cosmochim. Acta*, *54*, 575–590.

Stumm, W., and J. J. Morgan (1981), *Aquatic Chemistry*, 2nd ed., 780 pp., Wiley-Interscience, Hoboken, N. J.

Truesdell, A. H., and B. F. Jones (1969), Ion association of natural brines, *Chem. Geol.*, *4*, 51–62.

Turner, D. R., and M. Whitfield (1987), An equilibrium speciation model for copper in sea and estuarine waters at 25°C including complexation with glycine, EDTA and NTA, *Geochim. Cosmochim. Acta*, *51*, 3231–3239.

Turner, D. R., M. Whitfield, and A. G. Dickson (1981), The equilibrium speciation of dissolved components in freshwater and seawater at 25°C and 1 atm pressure, *Geochim. Cosmochim. Acta*, *45*, 855–881.

Wanninkhof, R. (1992), Relationship between wind speed and gas exchange over the ocean, *J. Geophys. Res.*, *97*, 7373–7382.

Weiss, R. (1974), Carbon dioxide in water and seawater: The solubility of a non-ideal gas, *Mar. Chem.*, *2*, 203–215.

Wesely, M. L. (1989), Parameterization of surface resistances to gaseous dry deposition in regional-scale numerical models, *Atmos. Environ.*, *23*, 1293–1304.

Wesely, M. L., and B. B. Hicks (1977), Some factors that affect the deposition rates of sulfur dioxide and similar gases on vegetation, *J. Air Pollut. Control Assoc.*, *27*, 1110–1116.

Wexler, A. S., and S. L. Clegg (2002), Atmospheric aerosol models for systems including the ions H^+, NH_4^+, Na^+, SO_4^{2-}, NO_3^-, Cl^-, Br^-, and H_2O, *J. Geophys. Res.*, *107*(D14), 4207, doi:10.1029/2001JD000451.

Whitfield, M. (1975a), An improved specific interaction model for seawater at 25°C and 1 atmosphere total pressure, *Mar. Chem.*, *3*, 197–213.

Whitfield, M. (1975b), The extension of chemical models for sea water to include trace components at 25°C and 1 atm pressure, *Geochim. Cosmochim. Acta*, *39*, 1545–1557.

Wilson, P. F., C. G. Freeman, M. J. McEwan, D. B. Milligan, R. A. Allardyce, and G. M. Shaw (2001), Alcohol in breath and blood: A selected ion flow tube mass spectrometric study, *Rapid Commun. Mass Spectrom.*, *15*, 413–417.

Zhang, Y. (2000), A comparative review of inorganic aerosol thermodynamic equilibrium modules: Similarities, differences, and their likely causes, *Atmos. Environ.*, *34*, 117–137.

————————————

M. Z. Jacobson, Department of Civil and Environmental Engineering, Stanford University, Stanford, CA 94305-4020, USA. (jacobson@stanford.edu)